



**HAL**  
open science

## Four core properties of the human brain valuation system demonstrated in intracranial signals

Alizée Lopez-Persem, Julien Bastin, Mathilde Petton, Raphaëlle Abitbol, Katia Lehongre, Claude Adam, Vincent Navarro, Sylvain Rheims, Philippe Kahane, Philippe Domenech, et al.

### ► To cite this version:

Alizée Lopez-Persem, Julien Bastin, Mathilde Petton, Raphaëlle Abitbol, Katia Lehongre, et al.. Four core properties of the human brain valuation system demonstrated in intracranial signals. *Nature Neuroscience*, 2020, 23 (5), pp.664-675. 10.1038/s41593-020-0615-9 . hal-02881927

**HAL Id: hal-02881927**

**<https://hal.sorbonne-universite.fr/hal-02881927>**

Submitted on 26 Jun 2020

**HAL** is a multi-disciplinary open access archive for the deposit and dissemination of scientific research documents, whether they are published or not. The documents may come from teaching and research institutions in France or abroad, or from public or private research centers.

L'archive ouverte pluridisciplinaire **HAL**, est destinée au dépôt et à la diffusion de documents scientifiques de niveau recherche, publiés ou non, émanant des établissements d'enseignement et de recherche français ou étrangers, des laboratoires publics ou privés.

# Four core properties of the human brain valuation system demonstrated in intracranial signals

## *Author List and affiliations*

Alizée Lopez-Persem<sup>\*(1,2)</sup>, Julien Bastin<sup>(3)</sup>, Mathilde Petton<sup>(4,5)</sup>, Raphaëlle Abitbol<sup>(1,2)</sup>, Katia Lehongre<sup>(2)</sup>, Claude Adam<sup>(2,6)</sup>, Vincent Navarro<sup>(2,6)</sup>, Sylvain Rheims<sup>(4,5,7)</sup>, Philippe Kahane<sup>(3,8)</sup>, Philippe Domenech<sup>(2,9,10,11)</sup>, Mathias Pessiglione<sup>\*(1,2)</sup>

(1) Motivation, Brain and Behavior team, Institut du Cerveau (ICM), Paris, France

(2) ICM, INSERM UMRS 1127, CNRS UMR 7225, Sorbonne Université, Paris, France

(3) Grenoble Institut Neuroscience (GIN), INSERM U1216, University of Grenoble Alpes, Grenoble, France

(4) Lyon Neuroscience Research Center, INSERM U1028, CNRS UMR5292, Lyon-Bron, France

(5) Université Claude Bernard Lyon 1, France

(6) AP-HP, Epilepsy Unit, INSERM U1028, CNRS UMR5292, Paris, France

(7) Department of Functional Neurology and Epileptology, Hospices Civils de Lyon and Lyon 1 University, Lyon, France

(8) CHU Grenoble Alpes, Grenoble, France

(9) Neurophysiology of Repetitive Behavior team, Institut du Cerveau (ICM), Paris, France

(10) Université Paris-Est Créteil, Créteil, France.

(11) CHU Henri Mondor, DMU Psychiatrie et d'Addictologie, Créteil, France

\* Corresponding authors: [lopez.alizee@gmail.com](mailto:lopez.alizee@gmail.com) and [mathias.pessiglione@gmail.com](mailto:mathias.pessiglione@gmail.com)

29

## *Abstract*

30

31 Estimating the value of alternative options is a key process in decision-making. Human fMRI  
32 and monkey electrophysiology studies have identified brain regions composing a valuation  
33 system, such as the ventromedial prefrontal and lateral orbitofrontal cortex (vmPFC and IOFC).  
34 Here, in an effort to bridge across species and techniques, we investigated the neural  
35 representation of value ratings in 36 human patients, using intracranial electroencephalography.  
36 We found that subjective value was positively reflected in both vmPFC and IOFC high-  
37 frequency activity, plus several other brain regions, including the hippocampus. We then  
38 demonstrated that subjective value could be decoded (1) in pre-stimulus activity, (2) for various  
39 categories of items, (3) even during a distractive task and (4) as both linear and quadratic signals  
40 (encoding both value and confidence). Thus, our findings specify key functional properties of  
41 neural value signals (anticipation, generality, automaticity, quadraticity), which might provide  
42 insights into human irrational choice behaviors.

43

44

## *Brief summary*

45 Lopez-Persem et al. used intracranial recordings in human patients to uncover key functional  
46 properties of neural value signals that might explain irrational choice behavior.

47

48

## *Introduction*

49

50 Standard decision-making theory assumes that making a choice involves two steps: first  
51 estimating the value of alternative options and then comparing these values to select the best  
52 option. While neural and computational models have been suggested for the value comparison  
53 process<sup>1,2</sup>, the value estimation process remains poorly understood<sup>3,4</sup>. Subjective values can be  
54 inferred from choice tasks, when several options are available, or elicited more directly using  
55 judgement tasks, when a single option is rated on a likeability scale<sup>5</sup>.

56 In the last decade, numerous studies, using either choice or rating tasks, have concurred to  
57 delineate a set of brain regions reflecting subjective values, termed brain valuation system  
58 (BVS)<sup>6</sup>. Meta-analysis of fMRI studies in humans have designated the ventromedial prefrontal  
59 cortex (vmPFC), the ventral striatum (vS) and the posterior cingulate cortex (pCC) as key  
60 components of the BVS<sup>7,8</sup>. However, many other brain regions have been reported to signal  
61 subjective values in particular fMRI studies. For instance, the hippocampus might critically

62 contribute to valuation when it involves imagining what the outcome would be like<sup>8,9</sup>. This is  
63 in accordance with the well-established notion that the hippocampal cortex (HC) can provide  
64 information stored in memory when a hypothetical episode needs to be assembled<sup>10,11</sup>. Also,  
65 the lateral part of the orbitofrontal cortex (IOFC) has been implicated in cue-outcome  
66 association paradigms involving reward and punishment<sup>12,13</sup>. Interestingly, other approaches  
67 such as intracranial single-cell recordings in monkeys have identified neurons reflecting  
68 subjective values not only in the vmPFC<sup>14,15</sup>, but also in many other brain regions, notably the  
69 IOFC<sup>16,17</sup>. Consistently, a recent study using electrocortigraphy (ECoG) electrodes placed on  
70 the cortical surface have described reward-related activity in the human IOFC during a  
71 gambling task<sup>18</sup>.

72 In an effort to bridge across techniques and species, we investigated the human brain with  
73 intracranial electro-encephalography (iEEG), which gives access to local field potentials in  
74 deep structures of the human brain. Thus, iEEG recordings avoid the attenuation and spatial  
75 diffusion of electric signals that are collected with scalp electrodes. Also, contrary to  
76 hemodynamic signals recorded with fMRI, they offer much better temporal resolution  
77 (milliseconds instead of seconds). Such recordings can be obtained in patients with drug-  
78 resistant focal epilepsy, who are implanted with intracranial electrodes for up to two weeks  
79 before surgery. This period provides a unique window into iEEG dynamics during performance  
80 of cognitive tasks in humans.

81 A first aim of our study was to identify which brain regions and which frequency bands were  
82 involved in generating value signals detectable with deep electrophysiology in humans.  
83 Contrary to typical electrophysiology studies, we did not select a priori the regions where  
84 electrodes were implanted, and collected data from 4273 recording sites, disseminated  
85 throughout the brains of 36 patients. A second aim was to compare the functional properties of  
86 these value signals with those previously described in fMRI studies. We focused on four core  
87 properties, which can be elicited with judgment tasks. These tasks, virtually impossible to  
88 implement in monkeys, have the advantage of presenting one item per trial, which facilitates  
89 tracking of value representations in brain activity, compared to choice tasks presenting two  
90 options or more.

91 All four functional properties have been identified from fMRI signals recorded in the vmPFC,  
92 and occasionally found in other BVS regions such as the vS, HC and pCC. First, the value  
93 signal recorded in the BVS depends on pre-stimulus baseline activity, which itself depends on  
94 the pleasantness of the internal or external context (e.g., mood level or background music)<sup>19,20</sup>.

95 Second, the BVS can assign values to different categories of objects, such as food, money,  
96 trinkets, faces, paintings, houses, charities etc.<sup>21,22</sup>, in accordance with the idea of a common  
97 neural currency<sup>23</sup>. Third, the BVS expresses subjective value in an automatic manner, meaning  
98 even if subjects are engaged in a distractive task<sup>22</sup>, or passively viewing choice options<sup>24</sup>.  
99 Fourth, the BVS not only reflects option or decision value, but also confidence in the judgment  
100 or choice<sup>25,26</sup>.

101 These properties are important because, taken together, they might explain some irrational  
102 judgements, such as the well-known misattribution bias (when distractors affect the value of  
103 target features) or the desirability bias (when expected value affects confidence). Indeed, these  
104 biases might arise from interference or spill-over effects, due to the fact that value and  
105 confidence relating to various features are automatically represented in the same neural  
106 substrates, whose activity may affect subsequent judgement or choice.

107 In order to assess the functional properties of value representation, we used different categories  
108 of items (food, faces, paintings), value-based and non-value-based first-order judgments  
109 (likeability and age ratings), and second-order judgments (confidence ratings). We first  
110 identified value signals across brain regions and frequency domains. Then we focused on  
111 regions of interest (ROI), not only those typically found in meta-analyses of fMRI studies (such  
112 as the vmPFC), but also others (such as the IOFC and HC) that together constitute the BVS. In  
113 each of these ROI, we tested whether the value signal would be anticipatory (predicting  
114 likeability rating in a pre-stimulus time window), generic (signaling the values of both food and  
115 non-food items), automatic (signaling value during the age rating task) and quadratic (reflecting  
116 confidence across first-order ratings).

117

## 118 *Results*

119

### 120 Behavior: linking value to choice, confidence and response time

121 36 patients suffering from epilepsy ( $37.9 \pm 10.7$  years old, 21 females, see demographical  
122 details in Supplementary Table 1) performed a series of rating and choice tasks (Figure 1a-c).  
123 One subset of patients (n=22) performed a short version of the behavioral tasks that only  
124 contained food items. In a first block, they had to rate the likeability of all food items presented  
125 one by one. In a second block, they had to choose between items of the same pool, now  
126 presented in pairs, according to their subjective preference. The other subset of patients (n=14)  
127 performed a long version of the same behavioral tasks, which added three components. First,

128 two other categories of items were included (faces and paintings) to assess the generality of  
129 value signaling. Second, a distractive task, in which patients rated the age of faces and paintings,  
130 was inserted to assess the automaticity of value signaling. Third, a confidence rating task was  
131 added on top of age and likeability ratings, in order to test the quadratic link between the two  
132 levels (first-order and second-order) of ratings. The two additional categories (face and  
133 painting) were also inserted in the choice task to check the relationship between likeability  
134 rating and pairwise preference. Trials were blocked such that all choices were made between  
135 items from the same category. Note that the age rating task was always performed first in these  
136 patients, to avoid priming valuation processes with the likeability rating task. The choice task  
137 was always performed last, so the pairing of items could be adjusted on the basis of their  
138 likeability ratings (see methods). The distributions of ratings and response times are provided  
139 in Extended Data 1 and 2.

140 We first tested whether subjective values could predict rating confidence and RT (Figure 1d-e),  
141 in the subset of patients who performed the long version of the task (black dots), pooling non-  
142 food items (faces and paintings) to increase statistical power. Using individual-level polynomial  
143 regression followed by group-level two-sided t-tests on regression coefficients, we confirmed  
144 a quadratic (U-shaped) relationship between first-order (age and likeability) and second-order  
145 (confidence) ratings ( $\beta_{\text{quad}}=0.21\pm 0.03$ ,  $t(13)=6.36$ ,  $p=2.10^{-5}$ ). This quadratic link was significant  
146 for both food and non-food items and for both age and likeability rating tasks ( $\beta_{\text{quad/non-}}$   
147  $\text{food/age}=0.16\pm 0.04$ ,  $t(13)=4.62$ ,  $p=5.10^{-4}$ ;  $\beta_{\text{quad/non-food/like}}=0.30\pm 0.06$ ,  $t(13)=4.92$ ,  $p=3.10^{-4}$ ;  
148  $\beta_{\text{quad/food/like}}=0.38\pm 0.08$ ,  $t(13)=4.79$ ,  $p=4.10^{-4}$ ). Note that a linear term was included in the  
149 polynomial fit, but was only significant for confidence in age rating ( $\beta_{\text{lin/non-food/age}}=-0.14\pm 0.05$ ,  
150  $t(13)=-2.81$ ,  $p=0.01$ ), probably reflecting the fact that some ages were easier to rate than others.

151 We also observed a significant quadratic link (inverted U-shape,  $\beta_{\text{quad}}=-0.30\pm 0.06$ ,  $t(13)=-4.96$ ,  
152  $p=2.10^{-4}$ ) between first-order rating and rating RT (from item display to first button press). This  
153 quadratic link was significant for both types of items and for both types of judgments ( $\beta_{\text{quad/non-}}$   
154  $\text{food/age}=-0.48\pm 0.02$ ,  $t(13)=-2.53$ ,  $p=0.025$ ;  $\beta_{\text{quad/non-food/like}}=-0.34\pm 0.09$ ,  $t(13)=-3.66$ ,  $p=3.10^{-3}$ ;  
155  $\beta_{\text{quad/food/like}}=-0.33\pm 0.01$ ,  $t(13)=-2.93$ ,  $p=0.012$ ). The linear term included in the polynomial fit  
156 was not significant (all  $p>0.17$ ). We also tested the possibility of higher-order effects by  
157 including a cubic term in the polynomial regressor. Results were unchanged for the linear and  
158 quadratic terms, with the cubic term being non-significant in every case (all  $p>0.05$ ).

159 Next, we tested whether subjective values could predict preferences recorded in the choice task  
160 (Figure 1f), starting with behavioral data obtained from the short version (including food items

161 only) that was common to all 36 patients (red dots). Individual logistic regression of choice rate  
162 (in a left versus right frame) against decision value (left minus right item likeability rating)  
163 showed a significant link at the group level ( $\beta_{\text{Food}}=0.42\pm 0.07$ ,  $t(34)=6.4$ ,  $p=2.10^{-7}$ ). Linear  
164 regression of choice response time (RT) against unsigned decision value, which is taken as an  
165 inverse proxy for choice difficulty, was also significant ( $\beta_{\text{Food}}=-72.8\pm 14.0$ ,  $t(34)=-5.19$ ,  $p=9.10^{-6}$ ).  
166 We then applied the same regression analyses to data from tasks that were specific to the  
167 long version (black dots). Again, we found that signed decision value predicted choice rate  
168 ( $\beta_{\text{Non-Food}}=-125\pm 0.03$ ,  $t(13)=12.8$ ,  $p=6.10^{-8}$ ) and that unsigned decision value predicted choice  
169 RT ( $\beta_{\text{Non-Food}}=0.37\pm 19.8$ ,  $t(13)=-6.32$ ,  $p=6.10^{-5}$ ). When these analyses were applied to face and  
170 painting separately, the results were also significant (choice rate:  $\beta_{\text{Face}}=0.38\pm 0.05$ ,  $t(12)=7.34$ ,  
171  $p=1.10^{-5}$ ,  $\beta_{\text{Painting}}=0.48\pm 0.10$ ,  $t(13)=4.68$ ,  $p=4.10^{-4}$ ; choice RT:  $\beta_{\text{Face}}=-121\pm 22.2$ ,  $t(12)=-5.43$ ,  
172  $p=2.10^{-4}$ ,  $\beta_{\text{Painting}}=-113\pm 22.2$ ,  $t(13)=-5.09$ ,  $p=2.10^{-4}$ ) and no significant difference was  
173 observed between regression estimates when comparing the three categories of items two by  
174 two (all  $p>0.05$ ). We also verified that decision value was a significant predictor of choice in  
175 every individual patient for all three categories (all  $p<0.05$ ).

176

177 Altogether, they confirmed that likeability ratings provide reliable estimates of subjective value,  
178 being significant predictors of various behavioral measures such as choice, response time and  
179 confidence (see Figure 1d-f). In the following, we focus on brain activity recorded during the  
180 rating tasks (Figure 1a and 1b), in which only one visual item was on screen at a time, making  
181 it possible to isolate the neural correlates of its subjective value.

182

### 183 Intracranial EEG: localizing value signals, a pseudo whole-brain analysis

184 Among our 4273 contacts distributed over the 36 patients, we could analyze 3194 good-quality  
185 bipolar signals, located in 77 regions of the AAL atlas<sup>27</sup>, each with at least 9 recording sites  
186 (Figure 2, Supplementary Table 2). For this pseudo whole-brain analysis, we focused on high-  
187 gamma band activity (in the 50-150Hz a priori range), since it is assumed to provide a bridge  
188 between fMRI<sup>28,29</sup> and spiking activity<sup>30,31</sup>. High-gamma power was extracted from every  
189 recording site time-series and regressed at each time point against subjective value. We took  
190 likeability rating obtained for food items as the main proxy for subjective value, because it was  
191 collected in all our patients. For each brain region of the restructured AAL atlas, we tested the  
192 significance of regression estimates in a fixed-effect analysis (pooling sites across patients) with  
193 correction for multiple comparisons across time points through non-parametric cluster-level

194 statistics (see methods).

195 In the high-gamma frequency band, we found 18 ROIs (over 77 analyzed ROIs) showing a  
196 significant expression of subjective value, after correcting for multiple comparisons across  
197 ROIs, with more than 20% of significant recording sites (Supplementary Table 3). This set of  
198 significant ROIs included the medial, middle and superior orbitofrontal cortex (vmPFC and  
199 IOFC), bilaterally. Among other significant brain regions, we retained those showing strong  
200 bilateral value signaling: the hippocampus and para-hippocampal cortex (PHC), the anterior  
201 cingulate gyrus, the anterior fusiform area, the inferior temporal cortex and the inferior frontal  
202 opercularis.

203 In the main results reported below, we focus on the a priori regions of interest, namely the  
204 vmPFC, IOFC, hippocampus and PHC (see anatomical locations in Figure 3a, Extended Data  
205 3 and 4). These four regions are referred to as the BVS and analyzed as two sub-systems, the  
206 OFC (including vmPFC and IOFC) and the (P)HC (including hippocampal and para-  
207 hippocampal cortex). We checked that the recording sites in these four main ROIs were  
208 similarly distributed across patients (Extended Data 3). The other regions expressing significant  
209 value signals are analyzed in the same way, and the results are presented as Extended Data.  
210 Together, they form what we hereafter call ‘the extended BVS’ (highlighted in Supplementary  
211 Table 3).

212

### 213 Investigation of value signals across ROIs and frequency bands

214 In each ROI, we explored the other frequency bands to assess whether our prior on the  
215 high-gamma band was justified. We first performed a time-frequency analysis on the evoked  
216 response (time-locked on item onset), averaged across all sites in a given ROI (Figure 3b). The  
217 time-frequency pattern was similar between vmPFC and IOFC on the one hand, and between  
218 HC and PHC on the other hand. We noticed that in the OFC, the border between increase in  
219 high-gamma power and decrease in gamma power was around 70Hz, so we refined our prior  
220 on the high-gamma band (from 50-150 to 70-150Hz). We also checked that anatomical  
221 boundaries between vmPFC and IOFC were correctly positioned, by tracking value signals  
222 along the medio-lateral axis. The strongest value signals were indeed found around the center  
223 of each ROI (Extended Data 4).

224 In order to define a time-window of interest for the following analyses, we extracted the  
225 regression estimates of the vmPFC, IOFC, hippocampus and PHC from the pseudo-whole brain  
226 analysis, for each time point between -0.2 and 1.5s around item onset (Figure 3d). We observed



227 a significant association (cluster-corrected, see methods) in the 0.77-1.03s window for the  
228 vmPFC, 0.36-1.00s for the IOFC, 0.16-1.28s for the hippocampus and 0.39-0.94s for the PHC.  
229 Examination of time courses suggests that value signals emerged later in the vmPFC compared  
230 to other ROIs. To better specify the propagation of value signals, we conducted cross-  
231 correlation analyses (see supplementary information). In the following analyses (Figure 3c), we  
232 focus on the 0.5-1s post-stimulus time window, which approximately corresponds to increased  
233 regression estimates in the four ROIs, hence to the valuation stage.

234 We found significant value signal for the four ROI in both gamma (vmPFC:  $\beta=0.044\pm0.0076$ ,  
235  $t(72)=5.78$ ,  $p=2.10^{-7}$ ; IOFC:  $\beta=0.037\pm0.0063$ ,  $t(151)=5.57$ ,  $p=1.10^{-7}$ ; HC:  $\beta=0.0299\pm0.0058$ ,  
236  $t(139)=5.11$ ,  $p=1.10^{-6}$ ; PHC:  $\beta=0.036\pm0.011$ ,  $t(60)=3.46$ ,  $p=9.10^{-4}$ ; two-sided one-sample t-  
237 tests) and high-gamma band (vmPFC:  $\beta=0.029\pm0.010$ ,  $t(72)=2.89$ ,  $p=5.10^{-3}$ ; IOFC:  
238  $\beta=0.046\pm0.0075$ ,  $t(151)=6.09$ ,  $p=8.10^{-9}$ ; hippocampus:  $\beta=0.051\pm0.0073$ ,  $t(139)=6.94$ ,  $p=1.10^{-10}$ ;  
239 PHC:  $\beta=0.0289\pm0.011$ ,  $t(60)=2.59$ ,  $p=0.012$ ). However, there was a significant divide  
240 between these two high-frequency and the lower-frequency bands, in every ROI (vmPFC:  
241  $t(72)=3.99$ ,  $p=2.10^{-4}$ ; IOFC:  $t(151)=6.26$ ,  $p=4.10^{-9}$ ; HC:  $t(139)=6.13$ ,  $p=8.10^{-9}$ ; PHC:  
242  $t(60)=4.07$ ,  $p=1.10^{-4}$ ; two-sided one-sample paired t-tests).

243 To compare the contribution of the different frequency bands to value signals in the BVS  
244 (pooling the 4 ROIs), we regressed food likeability ratings against power in all frequency bands  
245 as separate regressors. The contribution of high-frequency bands were about 10 times that of  
246 lower frequency bands ( $\beta_{H\gamma}=0.254\pm0.032$ ,  $\beta_{\gamma}=0.122\pm0.015$ ,  $\beta_{\beta}=0.026\pm0.011$ ,  $\beta_{\alpha}=-0.06\pm0.016$ ,  
247  $\beta_{\theta}=-0.011\pm0.012$ ). To further check that low-frequency bands were not adding any information  
248 about subjective value, we compared GLMs including only high-gamma and gamma bands to  
249 all possible GLMs containing these high-frequency bands plus any combination of low-  
250 frequency bands. Bayesian model selection (see Methods) designated the high-frequency GLM  
251 as providing the best account of subjective value ( $Ef=0.83$ ,  $Xp=1$ ).

252 Thus, even if low-frequency activity was significantly related to subjective value, it carried  
253 redundant information relative to that extracted from high-frequency activity. Consequently, we  
254 only kept gamma and high-gamma bands (grouped into the 'high-frequency' range) for the  
255 investigation of functional properties. The ROI analysis just extends the expression of  
256 subjective value to the gamma band, and circumscribes its temporal occurrence (around 0.5-1s  
257 post-stimulus).

258 The same time-frequency investigation was conducted in supplementary ROIs composing the  
259 extended BVS (Extended Data 5). Although value signals were weaker in these regions, they

260 shared similar features. The regression of food likeability ratings against high-gamma activity  
261 revealed significant clusters in the 0.5-1s time window for all regions. In addition, significant  
262 positive links were only observed in gamma and high-gamma bands, and negative links in the  
263 theta and alpha bands. This pattern was globally true at the (pseudo) whole-brain level: positive  
264 associations with value were mostly observed in high-frequency bands and negative  
265 associations in low-frequency bands (Supplementary Tables 3-7).

### 266 Testing the core properties of value coding in the Brain Valuation System

267 In the following analyses, we tested whether the core properties of the BVS identified with  
268 fMRI (anticipation, generality, automaticity, quadratic coding) are also observable in iEEG  
269 activity. Note that all these tests are independent from the selection of anatomical ROI, which  
270 was based on the linear regression of post-stimulus time-series against food likeability ratings.  
271 Thus, we extended regression analyses to other time windows (pre-stimulus or pre-response),  
272 other categories (non-food items), other type of judgement (age rating) and other type of coding  
273 (quadratic).

274

#### 275 *Anticipation (baseline activity predicts value judgments)*

276 For this analysis, we included a pre-stimulus time window (-0.2-0s), in addition to the pre-  
277 defined post-stimulus time window (0.5-1s). As expected, the association with food likeability  
278 rating (Figure 4) was significant in the post-stimulus time window for both ROIs (OFC:  
279  $t(449)=10.28, p<10^{-22}$ , (P)HC:  $t(401)=9.46, p=2.73 \cdot 10^{-19}$ ; two-sided one-sample t-tests). In the  
280 pre-stimulus time window, regression estimates were significant in the OFC ( $t(449)=2.38,$   
281  $p=0.018$ ), but not in the (P)HC ( $t(401)=-1.57, p=0.12$ ). We noted that anticipatory value  
282 signaling was not observed when restricting the dataset to patients performing the long version  
283 of the task, but this is likely due to the reduction in statistical power.

284 Nevertheless, anticipatory value signaling was confirmed by a decoding analysis in which a  
285 classifier was trained to decode high versus low ratings (see methods and Extended Data 6). In  
286 the OFC, two time-windows showed significant decoding (pre-stimulus: from -0.192 to 0.032s,  
287  $p_{\text{corr}}=0.01$  and post-stimulus: from 0.352 to 1.104s,  $p_{\text{corr}}<0.01$ ), while in the (P)HC, only one  
288 time window showed significant decoding (post-stimulus: from 0.480 to 0.992s,  $p_{\text{corr}} <0.01$ ).

289 In order to better understand this effect, we conducted a tertian-split analysis of the raw high-  
290 frequency activity recorded in each ROI. Activity recorded between -0.2 and 1.5s was averaged  
291 separately for high and low rating trials, in each patient and ROI (Extended Data 7). The shift  
292 in pre-stimulus activity was mostly observed in the vmPFC, for likeability ratings (not age

293 ratings). As previously observed with fMRI<sup>19</sup>, the raw signal change was a post-stimulus  
294 decrease, which was less pronounced for high values. Interestingly, the temporal dynamics of  
295 the signal was somewhat different between high and low rating trials, with faster changes for  
296 high values, which could explain why the time-locked correlation with value was lost between  
297 0 and 0.4s after stimulus onset.

298

### 299 *Generality (evoked activity reflects value judgments for different categories of items)*

300 To investigate whether the BVS would signal subjective value across categories, we extended  
301 the linear regression to the likeability of non-food items, which were obtained in the subset of  
302 patients who performed the long version of behavioral tasks.

303

304 First, we checked whether the likeability of food items was represented in the electrodes of this  
305 subset of patients (63 and 73 recording sites in the OFC and (P)HC respectively), in the same  
306 time window (0.5-1s post-stimulus). We found significant regression estimates in each ROI  
307 (OFC:  $t(125)=4.25$ ,  $p=4.10^{-5}$ , (P)HC:  $t(145)=5.17$ ,  $p=8.10^{-7}$ ; two-sided one-sample t-tests).  
308 Thus, regression against food likeability rating gave similar results (Figure 5a) as observed in  
309 the whole dataset (225 and 201 recording sites in the OFC and (P)HC respectively).

310 Then, we conducted the same regression analysis against the likeability of non-food items  
311 (Figure 5b). We found significant regression estimates for each ROI (OFC:  $t(125)=2.62$ ,  
312  $p=0.01$ , (P)HC:  $t(145)=2.34$ ,  $p=0.02$ ; two-sided one-sample t-tests), confirming that they were  
313 signaling the value of items from different categories.

314

### 315 *Automaticity (evoked activity reflects value judgments during non value-related tasks)*

316 To assess whether the BVS would also reflect subjective value during a distractive task,  
317 we extended the linear regression against the likeability of non-food items to the power time-  
318 series recorded during age rating (Figure 6). Interestingly, we observed a trend for a negative  
319 association with subjective value ( $p_{\text{corr}}=0.062$ ) between 0.470s and 0.580s after stimulus onset  
320 in the OFC and a significant negative association between 0.238s and 0.814s in the (P)HC  
321 ( $p_{\text{corr}}<1.10^{-4}$ ). The negative association in the OFC was followed by a significant positive  
322 correlation with subjective value between 0.829s and 1.094s ( $p_{\text{corr}}=3.10^{-3}$ ). We splitted our time  
323 window of interest in two halves, given the dynamics observed in the OFC, and confirmed a  
324 negative association with value in the 0.5-0.75s time window in both ROIs (OFC:  $t(125)=-$   
325  $2.027$ ,  $p=0.045$ ; (P)HC:  $t(145)=-3.89$ ,  $p=2.10^{-3}$ ; two-sided one-sample t-tests). In the second

326 time window, we found a significant positive association with value in the OFC only (OFC:  
327  $t(125)=3.43$ ,  $p=8.10^{-4}$ ; (P)HC:  $t(145)=-0.93$ ,  $p=0.35$ ; two-sided one-sample t-tests).

328 Thus, the results confirm that the OFC and the (P)HC can reflect value judgments during non-  
329 value-related tasks. They also uncover a surprising negative value representation that was most  
330 prominent in the (P)HC. Note that the negative correlation is not an artefact due to a difference  
331 in the latency of the evoked response, as the tertian split shows an inversion of the response to  
332 high- and low-value stimuli (Extended Data 7). To control for a potential contamination of age  
333 rating by likeability, we orthogonalized the two regressors and conducted the same regression  
334 analysis against power time-series. There was no noticeable difference in the results, with the  
335 same difference between the two time windows.

336

### 337 *Quadratic coding (evoked activity reflects confidence judgments on ratings)*

338 To test whether the BVS would also reflect second-order judgments (confidence in first-  
339 order ratings), we extended the time window of interest to the entire trial, and used time locking  
340 to both stimulus onset and motor response (first button pressed to move the cursor along the  
341 scale). Power time-series recorded in the two ROIs and two frequency bands were regressed  
342 against second-order polynomial extensions of (non-food) likeability rating and (non-food) age  
343 rating, collected in the long version of behavioral tasks (Figure 7). We consider quadratic terms  
344 as proxies for confidence ratings, since they are both U-shaped functions of first-order rating  
345 (see behavioral results). Using this proxy enables comparing regression results with the short  
346 versions of behavioral tasks (Extended Data 8a), for which confidence ratings were not  
347 acquired.

348 In the following analyses, we kept the 0.5-1s post-stimulus time window of interest and added  
349 an equivalent -0.5-0s time window before first button press (Figure 7 and Extended Data 8).  
350 Regression estimates for the quadratic function of likeability rating were significant over the  
351 post-stimulus time window in both ROIs (OFC:  $t(125)=5.55$ ,  $p=2.10^{-7}$ ; (P)HC:  $t(145)=4.51$ ,  
352  $p=1.10^{-5}$ ; two-sided one-sample t-test) and over the pre-response time windows in the OFC  
353 ( $t(125)=4.86$ ,  $p=3.10^{-6}$ ), but not in the (P)HC ( $t(145)=0.34$ ,  $p=0.74$ ).

354 Together, those results indicate that both OFC and (P)HC high-frequency activity reflected  
355 quadratic likeability ratings. The interpretation as a confidence signal (and not a saliency signal)  
356 is confirmed by the significant links observed with quadratic age rating. Indeed, the regression  
357 against quadratic age rating revealed a significant association in the pre-response time window  
358 in both ROIs (OFC:  $t(125)=2.94$ ,  $p=4.10^{-3}$ , (P)HC:  $t(145)=2.80$ ,  $p=6.10^{-3}$ ; two-sided one-

359 sample t-tests). Those results are illustrated in Figure 7b and 7d, for which high-frequency  
360 bands (gamma and high-gamma) power time-series were extracted from the post-stimulus and  
361 pre-response time windows and binned according to likeability or age rating.

362 As a control, we replicated the analysis in patients who performed the short version of  
363 behavioral tasks (using food items only) and therefore could not have been primed by  
364 confidence judgments (Extended Data 8a). The quadratic term was significantly expressed in  
365 both time windows (post-stimulus: OFC:  $t(323)=4.43$ ,  $p=1.10^{-5}$ , (P)HC:  $t(255)=4.54$ ,  $p=9.10^{-6}$ ;  
366 pre-response: OFC:  $t(323)=5.36$ ,  $p=2.10^{-7}$ , (P)HC:  $t(255)=6.43$ ,  $p=6.10^{-10}$ ; two-sided one-  
367 sample t-tests). This result suggests that representation of confidence was not induced by the  
368 instruction to rate confidence, which was only present in the long version.

369 As another control, we pooled all judgments together (likeability and age rating) and regressed  
370 the signal against the quadratic function of ratings. We compared the results to a regression  
371 against actual confidence judgments for patients who performed the long version (Extended  
372 Data 8). The results were qualitatively similar, with stronger statistics in the OFC (squared first-  
373 order ratings, post-stimulus:  $t(125)=5.87$ ,  $p=4.10^{-8}$ ; pre-response:  $t(125)=5.88$ ,  $p=3.10^{-8}$ ;  
374 confidence ratings, post-stimulus:  $t(125)=5.05$ ,  $p=1.10^{-6}$ ; pre-response:  $t(125)=3.57$ ,  $p=5.10^{-4}$ ).  
375 This result validates the use of squared rating as a proxy for confidence. Note that significant  
376 links with (P)HC activity were also observed in all cases, although not consistently over the  
377 entire time windows (see Extended Data 8).

378  
379 Altogether, the four functional properties were found in the OFC. All but the anticipation  
380 property were also observed in the (P)HC (Table 1). For every property, we conducted two-by-  
381 two comparisons (between and within the BVS ROIs) of regression estimates averaged over  
382 the relevant time windows. Compared to the OFC, the (P)HC only differed regarding the  
383 anticipation property ( $t(850)=3.37$ ,  $p=1.10^{-3}$ , see Table 1). Importantly, there was no significant  
384 difference between vmPFC and IOFC, which therefore shared the same four core properties.  
385 The same properties were tested in the other regions of the extended BVS: none exhibited the  
386 anticipation property but all of them shared the quadratic coding property (Supplementary Table  
387 8).

388

## 389 *Discussion*

390

391 Using a large dataset of iEEG signals recorded in 36 patients with epilepsy during judgment

392 tasks, we provide information about the BVS regarding 1) its anatomical localization over the  
393 whole brain, 2) the dynamical of the different frequency bands, 3) the functional properties of  
394 value representation. In the following, we successively discuss these three lines of results.

395

### 396     Delineating the Brain Valuation System

397 Using direct regression of high-gamma activity against the likeability ratings assigned to food  
398 items, we found a large set of brain regions that was significantly reflecting subjective value.  
399 Some of these significant ROIs were part of the standard BVS defined from meta-analyses of  
400 fMRI studies (e.g., vmPFC), some corresponded to areas where single cells were found to  
401 express subjective value (e.g., IOFC) and some were less classically associated with valuation  
402 (e.g., hippocampus). The fact that value correlates were similar between vmPFC and IOFC fills  
403 a gap between human fMRI and monkey electrophysiology studies. Indeed, previous fMRI  
404 studies using similar stimuli did not report value signals in the IOFC. The present results show  
405 that the implication of the IOFC in value representation is not dependent on the training  
406 procedures or particular tasks used in monkeys, but on the recorded signal (hemodynamic  
407 versus electrophysiological activity).

408 Thus, high-gamma band power, which arguably reflects local neural activation<sup>32,33</sup>, seems to  
409 provide an interesting bridge between human fMRI activity and monkey spiking activity. Our  
410 results are in line with a recent study that reported correlates of reward prospect and receipt in  
411 the human OFC high-frequency activity<sup>18</sup>, using electrocortigraphy (ECoG). This study raised  
412 the question of why most fMRI studies failed to detect any linear link between value correlates  
413 and IOFC activity. We can only offer trivial explanations here, such as a higher variability in  
414 the location of activated voxels across participants, or a more stringent statistical threshold,  
415 related to correction for multiple comparisons over a high number of recorded voxels.

416 Here, Bonferroni-Holm correction<sup>34</sup> was less stringent, because it was based on the number of  
417 ROIs tested (and not the number of voxels). This might partly explain the rather long list of  
418 significant associations with subjective value. The issue is even more problematic in typical  
419 monkey studies, which investigate only one brain region at a time, and therefore do not correct  
420 for multiple comparisons. Indeed, many brain regions have been reported to reflect reward or  
421 value across publications<sup>35,36</sup>. In any case, the number of ROIs that were found to correlate with  
422 subjective value questions the anatomical specificity of the BVS. This anatomical spread could  
423 reflect some functional diversity. Of note, we may have mixed regions involved in the  
424 construction of subjective value and those influenced by subjective value. Further investigation

425 is thus needed to tease apart the functional role of the different brain regions associated with  
426 subjective value.

427 We also note that some classical BVS regions were not in our list of ROIs significantly  
428 reflecting subjective value. One obvious reason is that they were not covered in our sample of  
429 recording sites, as was the case for the ventral striatum and posterior cingulate cortex. More  
430 generally, the unequal sampling of the AAL atlas ROIs induces differences in the statistical  
431 power of the group-level analyses used to test regression. This is why we used the term ‘pseudo  
432 whole-brain’ and why the comparison between regions must be taken with caution.

433

### 434 Dynamics of value coding across frequency bands

435 We observed that subjective value was represented in high-gamma activity of both the OFC and  
436 (P)HC, as expected from the pseudo whole-brain analysis. When exploring lower frequencies,  
437 the correlation with subjective value was similar between gamma and high-gamma bands for  
438 all regions. The correlation was reduced or even negative in low-frequency bands, which we  
439 did not analyze further because they were not providing any additional information about  
440 subjective values. This finding provides further support to the a priori correspondence between  
441 the BOLD signal and high-frequency iEEG activity, since we never observed negative  
442 correlation between brain activity and likeability rating in our fMRI studies<sup>9,22</sup> using similar  
443 stimuli. We also noted that in this high-frequency band, the main response observed in the  
444 vmPFC is a reduced power, with an even stronger reduction for lower values. It is tempting to  
445 draw a link with the decrease in BOLD signal that is also observed in the vmPFC following  
446 stimulus presentation. Indeed, a typical finding in fMRI studies is that higher stimulus value  
447 corresponds to lesser deactivation in the vmPFC (see for example <sup>19</sup>).

448 Focusing on high-frequency bands, we could then examine the separation between the two OFC  
449 regions (vmPFC and IOFC) in space and time. Regarding space, we observed a drop in value  
450 regression estimates for recording sites situated on the border between the two regions, along  
451 the medio-lateral axis. This observation argues against a possible spatial contamination of  
452 signals arising from the two regions. Spatial contamination was not very plausible anyway, as  
453 the average distance between the two ROI centers was 2-3 cm, whereas LFP signals were shown  
454 to aggregate neural activity over less than a 1cm-diameter sphere<sup>37</sup>. Regarding time, we  
455 observed that value signals emerged earlier in the IOFC relative to the vmPFC, which could  
456 therefore be the final processing stage before selection of the motor response. The analysis of  
457 the circulation of information was however limited by the fact that we seldom had all regions



458 of interest implanted with electrodes in a same patient.

459

### 460 Functional properties of value coding

461 All core functional properties of value coding that were previously identified with fMRI were  
462 replicated here in the vmPFC, and extended to the IOFC high-frequency iEEG activity.

463 First, we found that subjective values were partially predicted by pre-stimulus OFC activity. A  
464 similar result has been recently obtained in both humans and monkeys<sup>19</sup>. The suggestion was  
465 that a boost in baseline activity would persist in the evoked activity, resulting in a higher signal  
466 and hence a higher value, supposing that value is encoded in the absolute activity level, not in  
467 the difference from baseline. Such mechanism would predict that the link with upcoming value  
468 persists between baseline and evoked response (i.e., between 0 and 0.5s post-stimulus). We  
469 observed that the correlation with value was momentarily lost in this period, but this could be  
470 due to high values accelerating the evoked response. This anticipation is an important property  
471 that makes value judgment dependent on pre-choice activity, which itself can be influenced by  
472 irrelevant contextual features. It may therefore account for psychological phenomena such as  
473 misattribution bias or carry-over effects, for instance why we like the food better when the  
474 music is pleasant, or why we buy lottery tickets on sunny days.

475 Second, we found that the value of both food and non-food items was represented not only in  
476 OFC, but also in (P)HC activity. This is in line with a wealth of fMRI studies showing that  
477 likeability of faces and paintings was correlated with the BVS, and in particular vmPFC  
478 activity<sup>22,38</sup>, but also other kinds of items<sup>39</sup>, trinkets<sup>21</sup> and money<sup>40</sup>, consistent with  
479 the notion of a ‘common neural currency’<sup>23</sup>. This notion is critical for the ability to compare  
480 values and choose between items belonging to seemingly incommensurable categories. It is  
481 also an important condition for the psychological phenomena mentioned above, which assumes  
482 that the values of different features share a same neural representation, which may occasion  
483 interferences. We note that regression estimates were lower for the value of non-food items, but  
484 this may come from a different range of values in the different categories, or different mapping  
485 from value to the rating scale. Although the range of rewards explored is less extensive than in  
486 humans, several electrophysiological studies in monkeys reported that OFC neurons are  
487 sensitive to the value of non-food items, such as faces of conspecific animals<sup>41,42</sup>.

488 Third, we found that subjective value was expressed in both the OFC and (P)HC activity even  
489 during the age rating task. This is replicating the result previously obtained with fMRI<sup>22</sup>, and  
490 confirms that valuation is a somewhat automatic process. By this we do not mean that the



491 valuation process is irrepressible, just that valuation does not need an explicit value-based rating  
492 or choice task to be triggered. Importantly, the age rating task was performed first, precluding  
493 a priming of valuation processes by the likeability rating task. Such automatic valuation might  
494 explain a series of ‘halo effects’ reported in the literature, where the values of irrelevant  
495 contextual features contaminate the judgment of target stimuli. We note however that the  
496 dynamics of value coding was different from that observed in likeability rating tasks, with an  
497 early (surprisingly) negative correlation, followed by the (expectedly) positive correlation, at  
498 least in OFC activity. The negative correlation may occur when subjects estimate the age of  
499 visual items, and presumably shifts the representation of subjective value to a different neural  
500 code. This task-induced recoding may explain why automatic valuation has not been observed  
501 in some other fMRI studies using particular decision-making tasks<sup>43,44</sup>. We speculate that  
502 electrophysiological recordings would reveal automatic value signals even in these particular  
503 paradigms.

504 Fourth, we found that both OFC and (P)HC activity followed not only linear but also quadratic  
505 function of subjective value. The linear link was only observed with likeability, not age rating,  
506 confirming the implication of the BVS in valuation, not in assigning a number on a scale.  
507 Contrary to the linear link, the quadratic link was observed with both age and likeability ratings,  
508 and in both stimulus-locked and response-locked activity. This is consistent with the notion that  
509 the quadratic association represents confidence, defined as subjective accuracy of the response,  
510 as suggested in our previous fMRI study<sup>26</sup>. Indeed, we verified that confidence ratings were  
511 similarly represented in both stimulus-locked and response-locked activity. In other words, the  
512 BVS would represent both a first-order value judgment on the stimulus, and a second-order  
513 value judgment on the response. This implies that confidence carries an intrinsic value, as we  
514 prefer to be accurate than inaccurate. It is in line with a computational model postulating that  
515 confidence is precisely the quantity that subjects maximize when giving their response<sup>26</sup>.  
516 Confidence itself might be a generic and automatic process, as quadratic association was  
517 observed for both age and likeability ratings, even in subjects who were not asked to rate their  
518 confidence. This finding is consistent with animal studies claiming that OFC neurons represent  
519 confidence, which regulates how much they are willing to wait for the reward that they believe  
520 is associated to their response<sup>45</sup>. The co-occurrence of value and confidence representations in  
521 the same region may occasion some misattribution, as seen for instance in certain forms of  
522 desirability bias (when people feel more confident in their behavior just because the outcome  
523 is more rewarding).

524

525

### Limitations

526 To our knowledge, this is the first time that the BVS functional properties are investigated  
527 through intra-EEG recordings. However, these data have been collected in patients with  
528 epilepsy, who were investigated with depth electrodes for a presurgical evaluation. Yet we  
529 interpret those data as if they were collected in healthy subjects, making the assumption that  
530 epileptic activity did not distort the neural implementation of subjective value. Although we  
531 carefully rejected contacts and trials with epileptic activity, this assumption might be  
532 questionable. What is reassuring is that most of the results are in accordance with previous  
533 investigations in healthy human and non-human primates. Moreover, we investigated patients  
534 with different forms of epilepsy, which would induce disparate, or even opposed, distortions of  
535 brain activity, unlikely to explain systematic effects. Despite these limitations, we hope that  
536 further research will use the opportunity of iEEG recordings to improve our understanding of  
537 how subjective value is constructed in the human brain.

538

539

### *Acknowledgements*

540 We thank Jean-Philippe Lachaux, Marwa El Zein, Sebastien Bouret and Emmanuel  
541 Procyk for their helpful comments on the analysis of iEEG data, and the ICM for purchasing  
542 the acquisition material. This work benefited from the program 'Investissements d'avenir'  
543 (ANR-10-IAIHU-06), from the European Union's Horizon 2020 Research and Innovation  
544 Programme under Grant Agreement No. 720270 (HBP SGA1) and No. 785907 (HBP SGA2),  
545 from the LABEX CORTEX (ANR-11-LABX-0042) of Université de Lyon, within the program  
546 "Investissements d'Avenir" (ANR-11-IDEX-0007), from IHU CESAME, within the program  
547 "Investissements d'Avenir" (ANR-10-IBHU-0003) and from University Grenoble Alpes,  
548 within the program "Investissements d'Avenir" (ANR-17-CE37-0018 and ANR-18-CE28-  
549 0016). A.L-P. received a PhD fellowship from the Direction Générale de l'Armement and a  
550 grant from the LabEx Bio-Psy. The funders had no role in study design, data collection and  
551 analysis, decision to publish or preparation of the manuscript.

552

553

### *Author contributions*

554

555 M.Pes. designed all experiments. A.L-P., J.B. M.Pet. and R.A. collected the data. J.B. provided  
556 preprocessing scripts. A.L-P. performed the data analysis. C.A., V.N., S.R. and P.K. did the  
17

557 intracranial investigation and allowed the collection of iEEG data. K.L. supervised the access  
558 to patients in Paris. P.D. provided tools for time-frequency analysis. A.L-P. and M.Pes. wrote  
559 the manuscript. All authors discussed the results and commented the manuscript.

560

### 561 *Competing interests*

562

563 The authors declare no competing interests.

564

### 565 *References for main text only*

- 566 1. Krajbich, I., Armel, C. & Rangel, A. Visual fixations and the computation and comparison of value in simple  
567 choice. *Nat. Neurosci.* **13**, 1292–1298 (2010).
- 568 2. Hunt, L. T. *et al.* Mechanisms underlying cortical activity during value-guided choice. *Nat. Neurosci.* **15**, 470-  
569 S3 (2012).
- 570 3. O’Doherty, J. P. The problem with value. *Neurosci. Biobehav. Rev.* (2014)  
571 doi:10.1016/j.neubiorev.2014.03.027.
- 572 4. Juechems, K. & Summerfield, C. Where Does Value Come From? *Trends Cogn. Sci.* **23**, 836–850 (2019).
- 573 5. Lopez-Pessem, A., Rigoux, L., Bourgeois-Gironde, S., Daunizeau, J. & Pessiglione, M. Choose, rate or  
574 squeeze: Comparison of economic value functions elicited by different behavioral tasks. *PLOS Comput. Biol.*  
575 **13**, e1005848 (2017).
- 576 6. Rangel, A., Camerer, C. & Montague, P. R. A framework for studying the neurobiology of value-based  
577 decision making. *Nat. Rev. Neurosci.* **9**, 545–556 (2008).
- 578 7. Bartra, O., McGuire, J. T. & Kable, J. W. The valuation system: A coordinate-based meta-analysis of BOLD  
579 fMRI experiments examining neural correlates of subjective value. *NeuroImage* **76**, 412–427 (2013).
- 580 8. Peters, J. & Büchel, C. Episodic Future Thinking Reduces Reward Delay Discounting through an  
581 Enhancement of Prefrontal-Mediotemporal Interactions. *Neuron* **66**, 138–148 (2010).
- 582 9. Lebreton, M. *et al.* A Critical Role for the Hippocampus in the Valuation of Imagined Outcomes. *PLoS Biol.*  
583 **11**, e1001684 (2013).
- 584 10. Schacter, D. L., Addis, D. R. & Buckner, R. L. Remembering the past to imagine the future: the prospective  
585 brain. *Nat. Rev. Neurosci.* **8**, 657–661 (2007).
- 586 11. Barron, H. C., Dolan, R. J. & Behrens, T. E. J. Online evaluation of novel choices by simultaneous  
587 representation of multiple memories. *Nat. Neurosci.* **16**, 1492–1498 (2013).
- 588 12. O’Doherty, J., Kringelbach, M. L., Rolls, E. T., Hornak, J. & Andrews, C. Abstract reward and punishment  
589 representations in the human orbitofrontal cortex. *Nat. Neurosci.* **4**, 95–102 (2001).
- 590 13. Zhang, Z. *et al.* Distributed neural representation of saliency controlled value and category during anticipation  
591 of rewards and punishments. *Nat. Commun.* **8**, 1907 (2017).
- 592 14. Bouret, S. & Richmond, B. J. Ventromedial and Orbital Prefrontal Neurons Differentially Encode Internally  
593 and Externally Driven Motivational Values in Monkeys. *J. Neurosci.* **30**, 8591–8601 (2010).
- 594 15. Strait, C. E., Blanchard, T. C. & Hayden, B. Y. Reward Value Comparison via Mutual Inhibition in  
595 Ventromedial Prefrontal Cortex. *Neuron* **82**, 1357–1366 (2014).
- 596 16. Padoa-Schioppa, C. Orbitofrontal Cortex and the Computation of Economic Value. *Ann. N. Y. Acad. Sci.* **1121**,  
597 232–253 (2007).
- 598 17. Tremblay, L. & Schultz, W. Relative reward preference in primate orbitofrontal cortex. *Nature* **398**, 705–708  
599 (1999).
- 600 18. Saez, I. *et al.* Encoding of Multiple Reward-Related Computations in Transient and Sustained High-  
601 Frequency Activity in Human OFC. *Curr. Biol.* (2018) doi:10.1016/j.cub.2018.07.045.
- 602 19. Abitbol, R. *et al.* Neural Mechanisms Underlying Contextual Dependency of Subjective Values: Converging  
603 Evidence from Monkeys and Humans. *J. Neurosci.* **35**, 2308–2320 (2015).
- 604 20. Vinckier, F., Rigoux, L., Oudiette, D. & Pessiglione, M. Neuro-computational account of how mood  
605 fluctuations arise and affect decision making. *Nat. Commun.* **9**, 1708 (2018).
- 606 21. Chib, V. S., Rangel, A., Shimojo, S. & O’Doherty, J. P. Evidence for a Common Representation of Decision  
607 Values for Dissimilar Goods in Human Ventromedial Prefrontal Cortex. *J. Neurosci.* **29**, 12315–12320 (2009).
- 608 22. Lebreton, M., Jorge, S., Michel, V., Thirion, B. & Pessiglione, M. An Automatic Valuation System in the

- 609 Human Brain: Evidence from Functional Neuroimaging. *Neuron* **64**, 431–439 (2009).
- 610 23. Levy, D. J. & Glimcher, P. W. The root of all value: a neural common currency for choice. *Curr. Opin.*  
611 *Neurobiol.* (2012) doi:10.1016/j.conb.2012.06.001.
- 612 24. Levy, I., Lazzaro, S. C., Rutledge, R. B. & Glimcher, P. W. Choice from Non-Choice: Predicting Consumer  
613 Preferences from Blood Oxygenation Level-Dependent Signals Obtained during Passive Viewing. *J.*  
614 *Neurosci.* **31**, 118–125 (2011).
- 615 25. De Martino, B., Fleming, S. M., Garrett, N. & Dolan, R. J. Confidence in value-based choice. *Nat. Neurosci.*  
616 **16**, 105–110 (2013).
- 617 26. Lebreton, M., Abitbol, R., Daunizeau, J. & Pessiglione, M. Automatic integration of confidence in the brain  
618 valuation signal. *Nat. Neurosci.* **18**, 1159–1167 (2015).
- 619 27. Tzourio-Mazoyer, N. *et al.* Automated Anatomical Labeling of Activations in SPM Using a Macroscopic  
620 Anatomical Parcellation of the MNI MRI Single-Subject Brain. *NeuroImage* **15**, 273–289 (2002).
- 621 28. Logothetis, N. K., Pauls, J., Augath, M., Trinath, T. & Oeltermann, A. Neurophysiological investigation of  
622 the basis of the fMRI signal. *Nature* **412**, 150–157 (2001).
- 623 29. Scheeringa, R. *et al.* Neuronal Dynamics Underlying High- and Low-Frequency EEG Oscillations Contribute  
624 Independently to the Human BOLD Signal. *Neuron* **69**, 572–583 (2011).
- 625 30. Ray, S., Crone, N. E., Niebur, E., Franaszczuk, P. J. & Hsiao, S. S. Neural Correlates of High-Gamma  
626 Oscillations (60–200 Hz) in Macaque Local Field Potentials and Their Potential Implications in  
627 Electrooculography. *J. Neurosci.* **28**, 11526–11536 (2008).
- 628 31. Bastin, J. *et al.* Direct recordings in human cortex reveal the dynamics of gamma-band [50–150Hz] activity  
629 during pursuit eye movement control. *NeuroImage* **63**, 339–347 (2012).
- 630 32. Jerbi, K. *et al.* Task-related gamma-band dynamics from an intracerebral perspective: Review and  
631 implications for surface EEG and MEG. *Hum. Brain Mapp.* **30**, 1758–1771 (2009).
- 632 33. Lachaux, J.-P., Axmacher, N., Mormann, F., Halgren, E. & Crone, N. E. High-frequency neural activity and  
633 human cognition: Past, present and possible future of intracranial EEG research. *Prog. Neurobiol.* **98**, 279–  
634 301 (2012).
- 635 34. Holm, S. A Simple Sequentially Rejective Multiple Test Procedure. *Scand. J. Stat.* **6**, 65–70 (1979).
- 636 35. Wallis, J. D. & Kennerley, S. W. Heterogeneous reward signals in prefrontal cortex. *Curr. Opin. Neurobiol.*  
637 **20**, 191–198 (2010).
- 638 36. Hunt, L. T. & Hayden, B. Y. A distributed, hierarchical and recurrent framework for reward-based choice.  
639 *Nat. Rev. Neurosci.* **18**, 172–182 (2017).
- 640 37. Buzsáki, G., Anastassiou, C. A. & Koch, C. The origin of extracellular fields and currents — EEG, ECoG,  
641 LFP and spikes. *Nat. Rev. Neurosci.* **13**, 407–420 (2012).
- 642 38. Harvey, A. H., Kirk, U., Denfield, G. H. & Montague, P. R. Monetary Favours and Their Influence on Neural  
643 Responses and Revealed Preference. *J. Neurosci.* **30**, 9597–9602 (2010).
- 644 39. Hare, T. A., Camerer, C. F. & Rangel, A. Self-Control in Decision-Making Involves Modulation of the vmPFC  
645 Valuation System. *Science* **324**, 646–648 (2009).
- 646 40. Kable, J. W. & Glimcher, P. W. The neural correlates of subjective value during intertemporal choice. *Nat.*  
647 *Neurosci.* **10**, 1625–1633 (2007).
- 648 41. Watson, K. K. & Platt, M. L. Social Signals in Primate Orbitofrontal Cortex. *Curr. Biol.* **22**, 2268–2273  
649 (2012).
- 650 42. Azzi, J. C. B., Sirigu, A. & Duhamel, J.-R. Modulation of value representation by social context in the primate  
651 orbitofrontal cortex. *Proc. Natl. Acad. Sci.* **109**, 2126–2131 (2012).
- 652 43. Grueschow, M., Polania, R., Hare, T. A. & Ruff, C. C. Automatic versus Choice-Dependent Value  
653 Representations in the Human Brain. *Neuron* (2015) doi:10.1016/j.neuron.2014.12.054.
- 654 44. Grabenhorst, F. & Rolls, E. T. Selective attention to affective value alters how the brain processes taste stimuli.  
655 *Eur. J. Neurosci.* **27**, 723–729 (2008).
- 656 45. Mainen, Z. F. & Kepecs, A. Neural representation of behavioral outcomes in the orbitofrontal cortex. *Curr.*  
657 *Opin. Neurobiol.* **19**, 84–91 (2009).

## 659 *Figure legends*

660

### 661 **Figure 1 – Behavioral tasks and results**

662 **Top.** Behavioral tasks. Successive screens show example trials. In the age rating task **(a)** of  
663 non-food items (faces or paintings, framed in dark grey), patients provided judgments using

664 analog scales between 0 and 80 years for the age of faces and between 1400 and 2000 years  
665 for the date of paintings. Confidence in the first-order rating was reported on a continuous  
666 scale going from ‘not at all confident’ to ‘totally confident’. In the likeability rating task (**b**),  
667 patients indicated on an analog scale how much they liked the item from -10 to 10. The item  
668 could be food (red frame) or non-food (face or painting, dark grey). In the choice task (**c**), two  
669 items presented in the rating tasks were displayed side by side on the screen and patients had  
670 to select the one they preferred. **Bottom**. Behavioral results. In the rating tasks, the quadratic  
671 link was positive between confidence and age or likeability rating (**d-e**, top), and negative  
672 between RT and age or likeability rating (**d-e**, bottom), for both food (red dots) and non-food  
673 (black dots) items. In the choice tasks, the difference between likeability ratings (option values  
674  $V$ ) predicted both choice rate (**f**, top) and choice RT (**f**, bottom), for both food (red dots) and  
675 non-food (black dots) items.  $n=X$  indicates the number of patients tested for each result.  
676 Diamonds show binned data averaged across patients. Error bars are inter-subject S.E.M.  
677 Lines corresponds to polynomial fit for **d** and **e**, logistic fit for top **f** and linear fit for bottom  
678 **f**.

679

## 680 **Figure 2 – Anatomical locations of recording sites in the whole dataset**

681 **Top**. Sagittal slices of a brain template on which were superimposed the approximate locations  
682 of recording sites in 36 epileptic patients. Each dot (2 by 2 voxels) represents one recording  
683 site (i.e., a bipole). **Bottom**. Axial slices of a brain template that represents all AAL areas  
684 including at least 9 recording sites. Color coding (from dark red to light yellow) indicates the  
685 number of recording sites in each dot (top) or each area (bottom).  $x$  and  $z$  coordinates refer to  
686 the MNI atlas.

687

## 688 **Figure 3 – Time-frequency investigation of the BVS evoked response**

689 **a**. Anatomical localization of the vmPFC (red, first row), IOFC (blue, second row),  
690 hippocampus (green, third row) and PHC (brown, fourth row). All  $N$  recording sites located  
691 in those areas were included in the ROI analysis. **b**. Time-frequency analysis of the evoked  
692 response following visual item onset (dashed vertical line) averaged over all  $N$  recording sites  
693 and all food likeability rating trials. Hotter colors indicate higher power. Horizontal dashed  
694 lines indicate boundaries between frequency bands that are investigated in panels **c** and **d**.  
695 Horizontal thick black line between 0.5 and 1 s indicates the time window investigated in  
696 panels **c**. **c**. Regression estimates of power against food likeability rating, averaged over the  
697 0.5-1 s window, for each frequency band defined in **b**. Center lines, center circles, box limits,  
698 whiskers and points of the box plots respectively represent median, mean, interquartile range,  
699 extreme data points and outliers of the data distribution from the  $N$  recording sites. Black stars  
700 indicate significance ( $p < 0.05$ ) of regression estimates (one-sample two-sided  $t$ -test) ‘+’  
701 indicates a trend with  $p = 0.06$ . **d**. Time course of regression estimates for the gamma and high-  
702 gamma frequency band. Solid (dashed) lines indicates mean (SEM) across power time series.  
703 Stars indicate significant time points (one-sample two-sided  $t$ -test after cluster-wise  
704 correction,  $p < 0.05$ ). Shaded areas highlight the time window of interest used in **c** and in  
705 following analyses.  $n$ =number of power time series.

706

## 707 **Figure 4 – Anticipation of value signaling during pre-stimulus period in the BVS.**

708 Left. Time course of the regression estimates of OFC (top, pooling vmPFC and IOFC) and  
709 (P)HC (bottom, pooling hippocampus and PHC) activity against food likeability rating. Solid

710 lines represent means across recording sites and high-frequency bands (gamma and high-  
711 gamma). Dashed lines represent SEM across power time series. Double arrows indicate the  
712 tested pre-stimulus time window. Stars indicate significance of regression estimates against 0  
713 (after cluster-wise correction); ns indicates non-significance. n is the number of power time  
714 series included in the analysis. Shaded areas indicate time windows used for statistical report  
715 in the text. Right. Regions of interest included in each time course. Red: vmPFC, blue: IOFC,  
716 green: hippocampus, brown: PHC.

717

### 718 **Figure 5 – Generality of value signaling in the BVS.**

719 **a.** Time course of regression estimates for OFC (top, purple) and (P)HC (bottom, yellow) high-  
720 frequency bands (gamma and high-gamma) activity against food item likeability rating, in the  
721 subset of patients who were administered the long version of behavioral tasks. **b.** Time course  
722 of regression estimates in the same ROIs and frequency bands, against non-food item (painting  
723 and face) likeability rating, recorded during the likeability rating task. This analysis is meant  
724 to assess the generality of value signaling (extending from food to non-food categories).  
725 Illustrative screens of the behavioral tasks (food item likeability rating, non-food item  
726 likeability rating) are depicted on the left side. Location of ROIs is illustrated on the right side.  
727 Shaded areas correspond to the time window of interest (divided in two halves). Dashed lines  
728 represent SEM across recording sites. Stars represent significance of regression estimates  
729 tested against 0 (two-sided one-sample t-test,  $p < 0.05$ , after cluster-wise correction). n is the  
730 number of power time series included in the analysis.

731

### 732 **Figure 6 – Automaticity of value signaling in the BVS**

733 Plots show time-resolved regression of OFC (top, purple) and (P)HC (bottom, yellow) high-  
734 frequency band (gamma and high-gamma) power time series against non-food item (painting  
735 and face) likeability rating, recorded during the age rating task. This analysis is meant to assess  
736 the automaticity of value signaling (expressed during judgement of orthogonal dimensions  
737 such as age). Illustrative screens of the behavioral tasks (food item likeability rating, non-food  
738 item likeability rating) are depicted on the left side. Location of ROIs is illustrated on the right  
739 side. Shaded areas correspond to the time window of interest (divided in two halves). Dashed  
740 lines represent SEM across recording sites. Stars represent significance of regression estimates  
741 tested against 0 after cluster-wise correction (two-sided one-sample t-test,  $p < 0.05$ , cluster  
742 correction, '+' indicates a trend with  $p = 0.06$ ). n is the number of power time series included  
743 in the analysis.

744

### 745 **Figure 7 – Quadraticity of value signaling in the BVS.**

746 High-frequency band (gamma and high-gamma) power time series extracted from the OFC  
747 ROI (pooling vmPFC and IOFC data) were regressed against non-food squared likeability  
748 (top) and squared age (bottom). **a.** Plots show the time course of regression estimates locked  
749 on stimulus onset (left) and first button press (right). Stars represent significance of regression  
750 estimates tested against 0 after cluster-wise correction (two-sided one-sample t-test,  $p < 0.05$ ).  
751 Shaded areas depict time windows for which statistical results are reported in the text. Solid  
752 (dashed) lines indicates mean (SEM) across recording sites. **b.** Plots show high-frequency  
753 power in the OFC as a function of likeability or age rating. Circles (error bars) represent the  
754 mean (SEM) of bins, solid (and dashed) lines represent the mean (and SEM) of second-order  
755 polynomial fit. Significant linear and quadratic regressors are indicated as red p-values above

756 the graphs (two-sided one-sample t-test). **n** indicates the number of time series used in each  
757 analysis. **c** and **d** are the same analyses as in a and b, applied to the (P)HC ROI (pooling  
758 hippocampal and para-hippocampal data).

759

760

761 **Table 1: Summary of the BVS functional properties**

762

		ANTICIPATION	GENERICITY	AUTOMATICITY		QUADRATICITY
				0.5 – 0.75s	0.75 -1s	
OFC	n	450	126	126	126	450
	mean	0.011	0.015	-0.012	0.022	0.018
	SEM	0.005	0.005	0.006	0.007	0.003
	df	449	125	125	125	449
	t	2.380	2.620	-2.027	3.430	6.69
	p	0.018	0.010	0.045	8.10 <sup>-3</sup>	7.10 <sup>-11</sup>
(P)HC	n	402	146	146	146	402
	mean	-0.007	0.012	-0.0241	-0.008	0.017
	SEM	0.004	0.005	0.006	0.009	0.003
	df	401	145	145	145	401
	t	-1.570	2.340	-3.892	-0.930	6.29
	p	0.120	0.020	2.10 <sup>-4</sup>	0.350	6.10 <sup>-10</sup>

OFC vs (P)HC	mean	0.021	0.017	0.012	0.012	0.006
	SEM	0.006	0.009	0.009	0.016	0.004
	df	850	270	270	270	850
	t	3.365	1.958	1.380	0.758	1.693
	p	0.001	0.051	0.169	0.449	0.091
	vmPFC vs lOFC	mean	0.004	-0.013	0.004	0.020
	SEM	0.009	0.012	0.013	0.015	0.006
	df	448	124	124	124	448
	t	0.415	-1.050	0.313	1.303	1.793
	p	0.678	0.296	0.755	0.195	0.074

763 The table provides summary statistics for each functional property tested separately (two-sided  
764 one-sample Student’s test) in OFC and (P)HC activity (top) and for two-by-two comparisons  
765 (linear mixed-effects models) between and within ROIs (bottom). Abbreviations: SEM:  
766 standard error of the mean; df, t, p: degree of freedom, t-value and p-value of the test. In bold  
767 are the significant results. Anticipation: test of food likeability regression estimates in the -  
768 0.2-0s pre-stimulus activity. Genericity: test of non-food likeability regression estimates in the  
769 0.5-1.0s post-stimulus activity. Automaticity: test of the non-food likeability regression  
770 estimates during the age rating task in the 0.5-0.75s and 0.75-1s time windows after the  
771 stimulus onset. Quadraticity: test of squared food likeability regression estimates during the  
772 food likeability rating task in the -0.5-0s time window before the response onset. n indicates  
773 the number of power time series included in the analysis.

774



775

## *Methods*

776

### Patients and recordings

777 All 36 patients ( $37.9 \pm 10.7$  years old, 21 females, see demographical details in Supplementary  
778 Table 1) were suffering from drug-resistant focal epilepsy and gave written, informed consent  
779 prior to their inclusion in the study. They were tested in three different epilepsy departments:  
780 Lyon (n=18), Grenoble (n=7) and Paris (n=11). In Lyon and Grenoble, the implantation of  
781 electrodes and the participation of patients to cognitive tasks received approval from the  
782 Institutional Review Board and by the National French Science Ethical Committee (CPP 09-  
783 CHUG-12, study 0907) and from the French National Agency for Medicines and Health  
784 Products Safety (ANSM no: 2009-A00239-48). Patients underwent intracerebral recordings by  
785 means of stereotactically implanted<sup>46</sup> multilead depth electrodes (sEEG). For each patient, 12  
786 to 18 semi-rigid electrodes were implanted depending on the patient; each electrode had a  
787 diameter of 0.8 mm and comprised 6 to 18 leads of 2 mm, 1.5 mm apart (Dixi, Besançon,  
788 France), depending on the target region. The electrode contacts were identified on each  
789 individual stereotactic scheme, and then anatomically localized using the proportional atlas of  
790 Talairach & Tournoux<sup>47</sup>, after linear-scale adjustment to correct for size differences between  
791 the patient's brain and the brain template in the Talairach atlas. Neuronal recordings were  
792 conducted using an audio–video-EEG monitoring system (Micromed, Treviso, Italy), which  
793 allowed simultaneous recording of 128 or 256 depth-EEG channels sampled at 512 Hz [0.1–  
794 200 Hz bandwidth]. One of the contact sites located in the white matter was used as a reference.  
795 In Paris, the implantation of electrodes and the participation of patients to cognitive tasks  
796 received approval from local ethic committee (CPP Paris VI, Pitié-Salpêtrière Hospital,  
797 INSERM C11-16). The electrodes (AdTech®, Wisconsin) were 4-12 platinum contact  
798 electrodes, 1mm diameter and 1.6mm length, with nickel-chromium wiring. Neural recordings  
799 were conducted with Neuralynx (ATLAS, Neuralynx®, Inc., Bozeman, MO). Spatial  
800 localizations were determined on the basis of postimplant computed tomography scans  
801 coregistered with preimplant 1.5T MRI scans. Placement of the electrodes was determined by  
802 clinical criteria. The reference electrode was defined as the one with least activity, if possible  
803 in the white matter. Signal was band-pass filtered between 0.1 Hz and 1000 Hz. Localization of  
804 electrodes has been recovered automatically using the Epiloc toolbox (Version V1) developed  
805 by the STIM (<http://pf-stim.cricm.upmc.fr/>) engineering facility in the ICM (Institut du Cerveau  
806 et de la Moelle épinière, ([http://icm-institute.org/fr/cenir-stim-stereotaxy-core-facility-  
807 techniques-images-models/](http://icm-institute.org/fr/cenir-stim-stereotaxy-core-facility-techniques-images-models/))<sup>48</sup>.

808 Before analysis, all signals were re-referenced to their nearest neighbor on the same electrode,  
809 yielding a bipolar montage.

810

### 811 Blinding and randomization

812

813 There is no comparison between groups or conditions in our design and therefore no need for  
814 randomization or blind testing. The tasks were performed in the same order by every patient,  
815 but sequence of item presentation was randomized.

816

### 817 Experimental tasks

#### 818 *Long version*

819 In Paris, patients performed the long version of behavioral tasks, which were programmed on  
820 a PC using Matlab 2013 and the Cogent 2000 (Wellcome Department of Imaging Neuroscience,  
821 London, UK) library of Matlab functions for stimulus presentation.

822 The long version of the task comprised three phases and all trials started with a fixation cross  
823 lasting for  $1500 \pm 500$  ms.

824 First was the “Age Rating & Confidence task”, composed of 120 trials divided in two blocks  
825 of 60 trials (one with faces and the other with paintings), whose order was counterbalanced  
826 across patients. On every trial, an image appeared on screen and patients had to rate how old  
827 the presented stimulus was, on a 21-step scale that was adapted to the stimulus category (face  
828 or painting). After validation of the age judgment, another 100-step (almost continuous) rating  
829 scale was displayed, on which participants were asked to indicate how confident they were,  
830 between “Not at all” and “Totally”, about their first-order rating, which was reminded on the  
831 screen (“You gave a rating of  $X$ ”). In all rating tasks, the answer was given with the right hand.

832 The cursor initial position was randomized and it could be moved by pressing left and right  
833 arrows on the keyboard and then validated by pressing the space bar. Once validated, the next  
834 trial started. The order of stimulus presentation was randomized, separately for each participant.

835 Second, in the “Likeability Rating & Confidence task”, patients were shown in three different  
836 blocks the same faces and paintings, with the addition of a block presenting food items (60 trials  
837 in each block). They were asked to indicate on a 21-step scale graduated from -10 to 10 how  
838 much they liked the stimulus presented on screen. Each likeability rating was followed by a  
839 confidence rating, presented in the same way as during the age rating task.

840 Third, patients completed three blocks of 60 trials each of a forced binary choice task among  
841 the stimuli that were previously rated. After the fixation cross, two pictures belonging to the  
842 same category (food, face or painting) were displayed on each side of the screen. Patients had  
843 to choose the one they preferred by pressing the left or right arrow of the keyboard. The selected  
844 option was framed to give patients a visual feedback on their choice. Note that one patient did  
845 not complete the tasks on face stimuli (age, likeability and choice) but we nonetheless included  
846 his data in the analysis.

#### 847 *Short version*

848 In Lyon and Grenoble, patients performed the short version of behavioral tasks, composed of  
849 one likeability rating task without confidence judgment and one binary choice task, both  
850 restricted to food items. All food stimuli were displayed using Presentation software (version  
851 16.5, Neurobehavioral Systems, Albany, CA) on a 17 CRT monitor at 85 Hz. The EEG-  
852 acquisition PC was synchronized to the stimulation PC via a TTL pulse signaling stimulus  
853 onset. All aspects of the food rating and choice tasks were the same as previously described,  
854 except that they completed 120 trials for each task instead of 60. The order of stimulus  
855 presentation was also randomized, separately for each participant. Note that one patient did not  
856 complete the choice task but we nonetheless included his rating task data in the analysis.  
857 3 patients in Grenoble completed the long version of the task, using the setup of the short  
858 version (Presentation software and 85 Hz monitor), but the experimental details of the long  
859 version. Among them, one completed both versions (short then long on another day).

#### 860 **Behavioral analysis**

861 Unless otherwise specified, all dependent variables (raw, *z*-scored or binned behavioral  
862 measures and regression estimates) were analyzed at the subject level and tested for significance  
863 at the group level (random-effect analysis) using two-tailed paired *t*-tests. All regressions were  
864 performed on *z*-scored independent and dependent variables. All variables were tested for  
865 normality using the Kolmogorov–Smirnov (K-S) test (all  $p > 0.05$ ). All statistical analyses were  
866 performed with Matlab Statistical Toolbox (Matlab R2016a, The MathWorks, Inc., USA).

#### 867 **Electrophysiological analysis**

868 Collected iEEG signals were analyzed with the software package for electrophysiological  
869 analysis (ELAN-Pack, Elan for Ubuntu-10-x86\_64) developed in Lyon (INSERM U1028,  
870 Lyon, France), with the addition of Fieldtrip<sup>49</sup> (version r7276,  
871 <http://www.ru.nl/neuroimaging/fieldtrip>) and homemade Matlab algorithms. Bipolar

872 derivations were computed between adjacent contacts to suppress contributions from non-local  
873 assemblies and ensure that iEEG signals could be considered as originating from a cortical  
874 volume centered within the two contacts<sup>32</sup>. 50 Hz noise was removed from the data using a  
875 notch filter. Data were then inspected in order to remove electrodes with suspected epileptic  
876 focus from the analysis: windows of 50 ms around time points with intensity higher or lower  
877 than five times the standard deviation of the average signal were replaced by NaN values, in  
878 order to exclude those points from the following analyses. Data normality was assessed with  
879 the Kolmogorov–Smirnov (K-S) test prior to any statistical test (all  $p > 0.05$ ).

880

### 881 *AAL restructuration*

882 The AAL (Automated Anatomical Labeling) Atlas was used to label each contact located in the  
883 MNI space. However, in order to get comparable size and hence statistical power, brain regions  
884 larger than 2000 voxels were separated in two brain regions along the larger axis (until all  
885 regions had a volume inferior to 2000 voxels). On the contrary, brain regions smaller than 1000  
886 voxels were combined (as for example the gyrus rectus or the frontal medial orbital brain area).  
887 We nevertheless kept some regions with less than 1000 voxels, because it would make no sense  
888 to combine them with their neighbors. These regions were the bilateral amygdala (220 voxels),  
889 the bilateral Heschl gyrus (225 voxels) and the bilateral pallidum (473 voxels). The new atlas  
890 included 115 areas (see Supplementary Table 2), with an average volume of 1771 +/- 124  
891 voxels. Only the 77 regions with at least 9 recording sites were retained for statistical analyses.  
892 Our dataset included a total of 4273 recording contacts in 36 patients. Contacts with low-quality  
893 signals were removed and bipolar montages were computed for each pair of adjacent contacts.  
894 Among the 3440 remaining recording sites, 3194 were located within one of these 77 regions  
895 and were therefore kept for analysis. Coordinates of recording sites were computed as the mean  
896 of the MNI coordinates of the two contacts composing the bipole.

897 The term ‘pseudo’ acknowledges the fact that comparison between regions is heavily biased by  
898 differences in the number of recording sites, which conditions the statistical power of the test  
899 performed to detect value signals.

900

### 901 *Regions of interest definition*

902 The vmPFC ROI (73 sites, in red on Figure 3a and Supplementary Table 2) was defined as the  
903 gyrus rectus plus the fronto-medial part of orbitofrontal cortex bilaterally. The IOFC ROI (152  
904 sites, in blue on Figure 3a and Supplementary Table 2) was defined as the bilateral central and

905 lateral parts of the orbitofrontal cortex (AAL labels: frontal superior orbital and frontal middle  
906 orbital, respectively). The hippocampus (140 sites) and PHC (61 sites) ROIs correspond to  
907 those defined in the AAL (in green and brown on Figure 3a, Supplementary Figure 3 and  
908 Supplementary Table 2).

909

#### 910 *Extraction of frequency envelopes*

911 To determine the time course of a priori high-gamma band power, continuous iEEG signals  
912 were first band-pass filtered in multiple successive 10Hz-wide frequency bands (e.g., 11 bands  
913 from [50–60 Hz] to [140–150 Hz]) using a zero-phase shift non-causal finite impulse filter with  
914 0.5 Hz roll-off. Next, for each band-pass filtered signal we computed the envelope using  
915 standard Hilbert transform. The obtained envelope had a sampling rate of 64 Hz (i.e., one time  
916 sample every 15.625 ms). Again, for each frequency band, this envelope signal (i.e., time  
917 varying amplitude) was divided by its mean across the entire recording session and multiplied  
918 by 100. This yields instantaneous envelope values expressed in percentage (%) of the mean.  
919 Finally, the envelope signals computed for each consecutive frequency band were averaged  
920 together to provide a single time series (the high-gamma band envelope) across the entire  
921 session. By construction, the mean value of that time series across the recording session is equal  
922 to 100. Note that computing the Hilbert envelopes in 10Hz sub-bands and normalizing them  
923 individually before averaging over the broadband interval allows us to counteract a bias toward  
924 the lower frequencies of the interval induced by the 1/f drop-off in amplitude. Finally, the  
925 obtained time series were smoothed using a sliding window of 250 ms to get rid of potential  
926 artifacts.

927 The envelopes of theta, alpha, beta and gamma bands were extracted in a similar manner as the  
928 high-gamma frequency except that steps were 1 Hz for theta and alpha and 5 Hz for beta and  
929 gamma. The ranges corresponding to the different frequency bands were determined according  
930 to the average time-frequency profiles observed across patients and contacts in the selected  
931 region of interest (see Figure 3). High-gamma band was defined as 70-150 Hz, gamma as 35-  
932 70 Hz, beta as 15-35 Hz, alpha as 8-15 Hz and theta as 4-8 Hz.

933

#### 934 *General Linear Models*

935 Frequency envelopes of each bipolar contact were epoched on each trial with two time locking  
936 (stimulus onset: -500 to 1500 ms, and first keypress: -1500 to 1500 ms). Each time series was  
937 regressed against the variables of interest to obtain a regression estimate per time point and

938 contact.

939 In all GLMs, power  $Y$  (normalized envelope) was regressed across trials against rating  $R$   
940 (normalized within patients and tasks  $R$ ) at every time point:

$$941 Y = \alpha + \beta R$$

942 With  $\beta$  corresponding to the regression estimate on which statistical tests are conducted.  $R$   
943 corresponds to:

944 - Food likeability rating during the likeability rating task in the figures 3, 4, and 5a, and  
945 Extended Data 4, 5, 6.

946 - Painting and face likeability rating during the likeability rating task in figure 5b

947 - Painting and face likeability rating during the age rating task in figure 6.

948 - Squared likeability, age and confidence ratings during likeability, age and confidence rating  
949 tasks in Figure 7 and Extended Data 8c (Judgment<sup>2</sup>)

950 - Confidence rating (on age and likeability rating) in Extended Data 8c (Confidence rating).

951 For the investigation of quadratic coding, each power time-series  $Y$  was regressed against  
952 second-order polynomial extensions of rating:

$$953 Y = \alpha + \beta_1 R + \beta_2 R^2$$

954 With  $\beta_1$  and  $\beta_2$  corresponding to the « linear term » and « quadratic term » regression estimates.

955 To assess the contribution of the different frequency bands to value representation, we  
956 used the following GLM:

$$957 R = \beta_{H\gamma} * Y(H\gamma) + \beta_{\gamma} * Y(\gamma) + \beta_{\beta} * Y(\beta) + \beta_{\alpha} * Y(\alpha) + \beta_{\theta} * Y(\theta)$$

958 With  $\beta$  corresponding to the regression estimates each power time series  $Y$  in the high-gamma,  
959 gamma, beta, alpha and theta frequency bands. This GLM was compared to the 7 following  
960 GLMs:

$$961 R = \beta_{H\gamma} * Y(H\gamma) + \beta_{\gamma} * Y(\gamma)$$

$$962 R = \beta_{H\gamma} * Y(H\gamma) + \beta_{\gamma} * Y(\gamma) + \beta_{\beta} * Y(\beta)$$

$$963 R = \beta_{H\gamma} * Y(H\gamma) + \beta_{\gamma} * Y(\gamma) + \beta_{\alpha} * Y(\alpha)$$

$$964 R = \beta_{H\gamma} * Y(H\gamma) + \beta_{\gamma} * Y(\gamma) + \beta_{\theta} * Y(\theta)$$

$$965 R = \beta_{H\gamma} * Y(H\gamma) + \beta_{\gamma} * Y(\gamma) + \beta_{\beta} * Y(\beta) + \beta_{\alpha} * Y(\alpha)$$

$$966 R = \beta_{H\gamma} * Y(H\gamma) + \beta_{\gamma} * Y(\gamma) + \beta_{\beta} * Y(\beta) + \beta_{\theta} * Y(\theta)$$

$$967 R = \beta_{H\gamma} * Y(H\gamma) + \beta_{\gamma} * Y(\gamma) + \beta_{\alpha} * Y(\alpha) + \beta_{\theta} * Y(\theta)$$

968 The model comparison was conducted using the VBA toolbox (version V3, Variational  
969 Bayesian Analysis toolbox, available at <http://mbb-team.github.io/>). Log-model evidence  
970 obtained in each recording site was taken to group-level random-effect Bayesian model

971 selection (RFX-BMS) procedure<sup>50,51</sup>. RFX-BMS provides an exceedance probability ( $X_p$ ) that  
972 measures how likely it is that a given model is more frequently implemented, relative to all the  
973 others considered in the model space, in the population from which samples were drawn.

974

#### 975 *Statistical assessment*

976 No statistical methods were used to pre-determine sample size but our sample size is much  
977 larger than those reported in typical publications using iEEG<sup>18,52</sup>.

978 For all GLMs, significance of regressors was assessed using one-sample two-tailed t-tests. T-  
979 values and p-values of those tests are reported in the results sections. Effect sizes correspond to  
980 standardized linear regression coefficients obtained with the matlab function `glmfit`. When  
981 comparing two regions, significance was assessed using linear mixed-effects models, that  
982 included patient ID as a random factor. When comparing frequencies, significance was assessed  
983 using a two-tailed paired t-test.

984 When no a priori time window was selected, significance was assessed through permutation  
985 tests. The pairing between power and regressor values across trials was shuffled randomly 2000  
986 times. The maximal cluster-level statistics (the sum of t-values across contiguous time points  
987 passing a significance threshold of 0.05) were extracted for each shuffle to compute a ‘null’  
988 distribution of effect size across a time window of -0.2 to 1.5 s around stimulus presentation, or  
989 -1 to 1 s around first keypress. For each significant cluster in the original (non-shuffled) data,  
990 we computed the proportion of clusters with higher statistics in the null distribution, which is  
991 reported as the ‘cluster-level corrected’ p-value ( $p_{\text{corr}}$ )<sup>53</sup>.

992

#### 993 *Whole-brain analysis*

994 For each region included in the pseudo whole-brain analysis, a t-value was computed across all  
995 recording sites for each time point after stimulus onset, independently of patient identity (fixed-  
996 effect second-level analysis). This allowed the inclusion of brain regions with a small number  
997 of recording sites. Significance of each brain region was assessed by permutation tests on  
998 clusters longer than 80 ms with a corrected  $p=0.05$ , as describe above. Significance threshold  
999 was then corrected for multiple comparisons across brain regions, using Bonferroni-Holm  
1000 correction. The minimal duration of a cluster was set in order to avoid any transitory false  
1001 positive effect.

1002



1003 *Time-frequency analysis*

1004

1005 Time-frequency analyses were carried out using the FieldTrip toolbox for MATLAB. Spectral  
1006 powers were estimated using a “multitapering” time-frequency transform (Slepian tapers,  
1007 lower frequency range: 4–32 Hz, 6 cycles and 3 tapers per window, higher frequency range: 32-  
1008 200 Hz, fixed time windows of 240 ms, 4 to 31 tapers per window). This approach uses a  
1009 constant number of cycles across frequencies up to 32 Hz (hence a time window whose duration  
1010 decreases when frequency increases), and a fixed time window with an increasing number of  
1011 tapers above 32 Hz to obtain more precise power estimates by adaptively increasing smoothing  
1012 at high frequencies.

1013

1014 *Cross-correlation analysis*

1015

1016 To assess the temporal dynamics of value representation across regions (Supplementary Figures  
1017 1 and 2), we searched for correlations between every possible combination of regression  
1018 estimates obtained for (non-smoothed) high-gamma band power against food likeability. All  
1019 possible pairs of electrodes implanted in a same patient were tested. For each pair, we computed  
1020 one Pearson’s correlation coefficient per time lag, from 0 to 0.5 s with steps of 16 ms (time  
1021 resolution of the preprocessed data). Correlation coefficients for a given pair of regions were  
1022 then tested for significance, pooling pairs recorded in different patients (fixed effect). The null  
1023 distribution of effect size was established using 1000 permutation of pair labels.

1024

1025 *Decoding analysis*

1026

1027 All high-frequency signals recorded in a given ROI during the food likeability rating  
1028 task were combined in large time by trial matrices. Trials were sorted into high and low ratings  
1029 using a tertian split. At every time point, a logistic classifier was trained on 90% of trials, and  
1030 tested on the remaining 10%, with 100 different partitions. The average accuracy per time point  
1031 is displayed in Extended Data 6. The same procedure was applied on 1000 label permutations  
1032 to get a random decoding score per time point. Cluster-correction was then applied on the time-  
1033 window showing significance.

1034 The tertian split was also used to assess the dynamics of high-gamma band evoked response  
1035 and displayed in Extended Data 7, first row. A similar procedure was applied to high-gamma



1036 signals recorded during the non-food age rating task and provided the results displayed in  
1037 Extended Data 7, second row.

1038

### 1039 *Data availability*

1040 The data that support the findings of this study are available from the corresponding author  
1041 (A.L-P.) upon request.

1042

### 1043 *Code availability*

1044 The custom code used to generate the figures and statistics are available from the corresponding  
1045 author (A.L-P.) upon request.

1046

### 1047 *Reporting Summary*

1048

1049 Further information on research design is available in the Life Sciences Reporting Summary  
1050 linked to this article.

1051

### 1052 *Methods-only references*

1053

1054 46. Lachaux, J. P., Rudrauf, D. & Kahane, P. Intracranial EEG and human brain mapping. *J. Physiol.-Paris* **97**,  
1055 613–628 (2003).

1056 47. Talairach, J. & Tournoux, P. Co-planar stereotaxic atlas of the human brain. 3-Dimensional proportional  
1057 system: an approach to cerebral imaging. (1988).

1058 48. Perez-Garcia, F. *et al.* Automatic segmentation of depth electrodes implanted in epileptic patients: a modular  
1059 tool adaptable to multicentric protocols. *Epilepsia* **56**, 227 (2015).

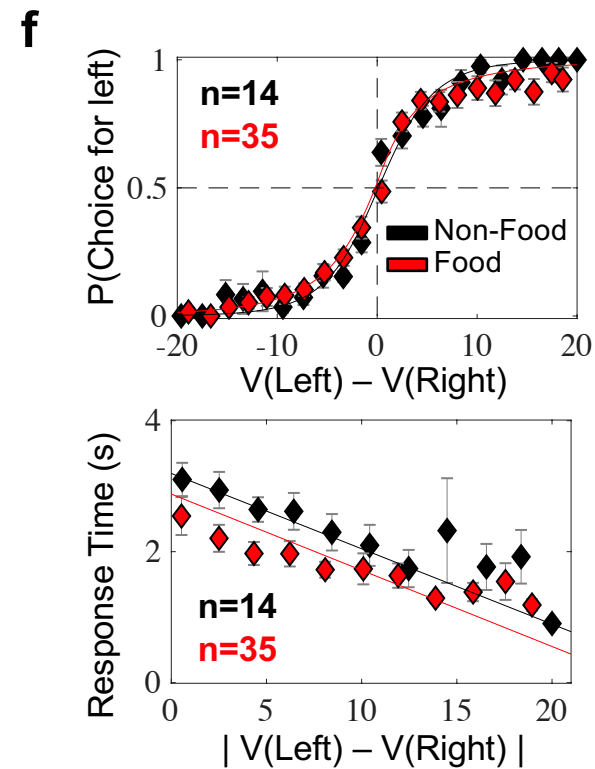
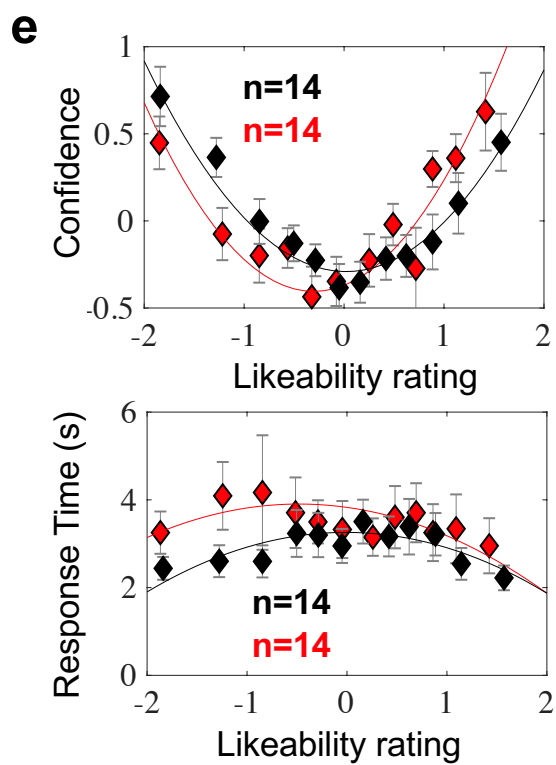
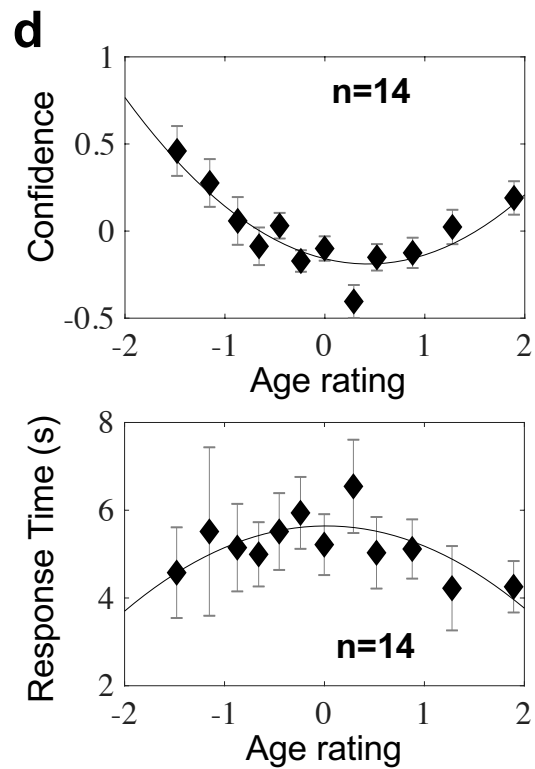
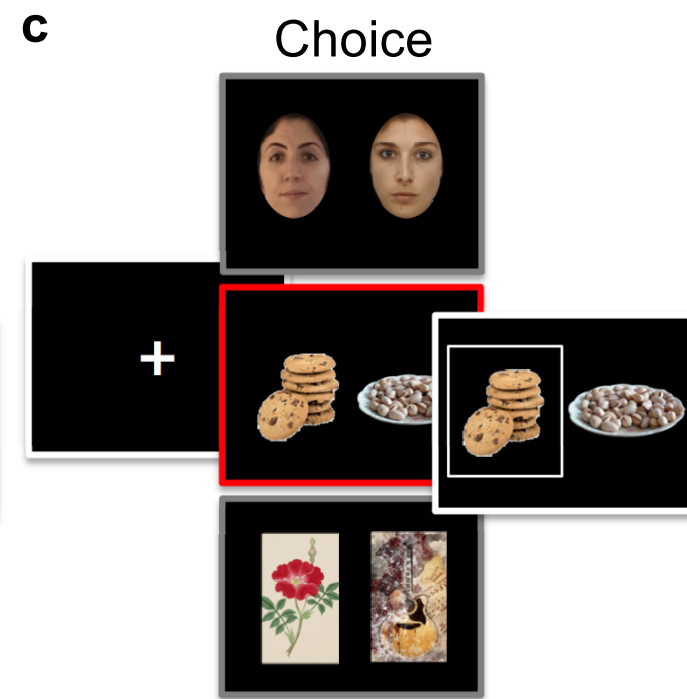
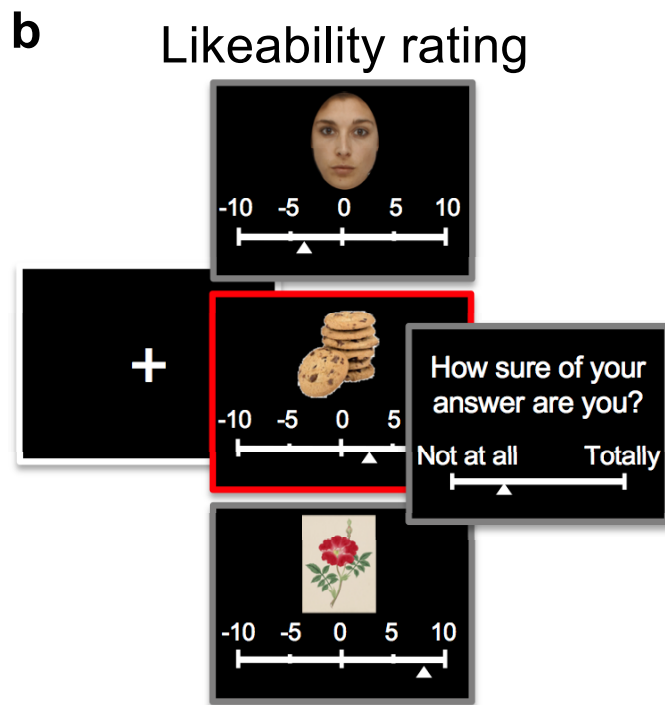
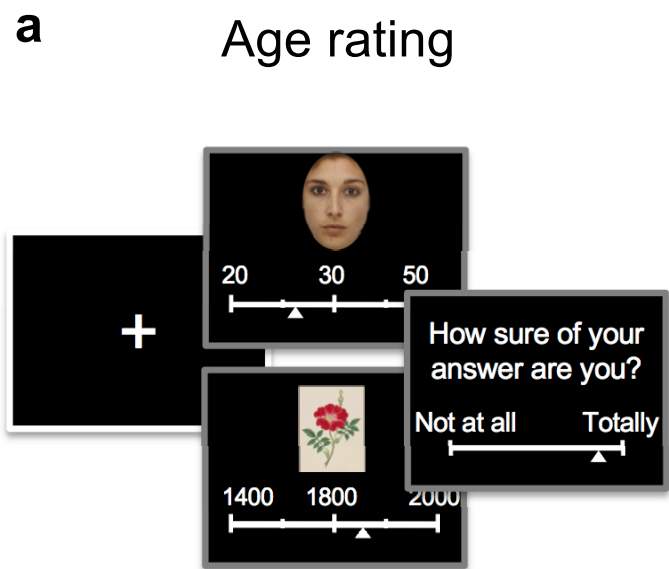
1060 49. Oostenveld, R., Fries, P., Maris, E. & Schoffelen, J.-M. FieldTrip: Open Source Software for Advanced  
1061 Analysis of MEG, EEG, and Invasive Electrophysiological Data. *Computational Intelligence and*  
1062 *Neuroscience* <https://www.hindawi.com/journals/cin/2011/156869/> (2011) doi:10.1155/2011/156869.

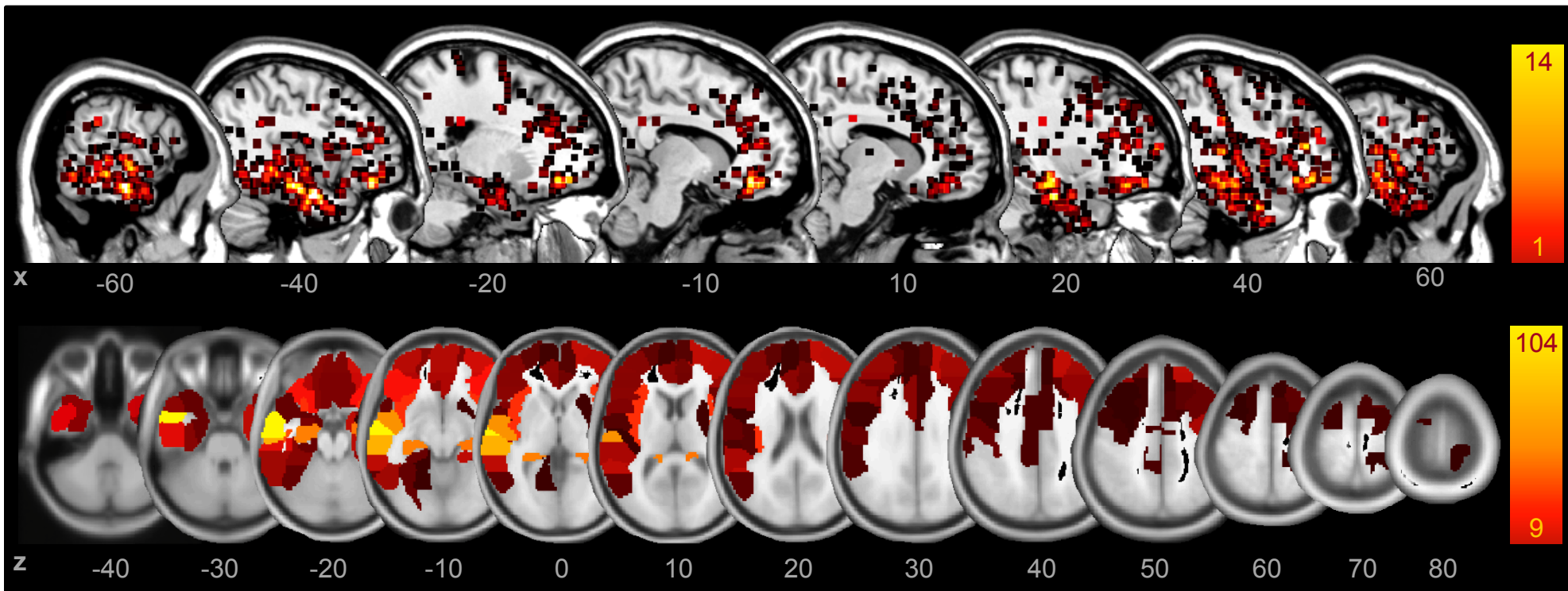
1063 50. Rigoux, L., Stephan, K. E., Friston, K. J. & Daunizeau, J. Bayesian model selection for group studies —  
1064 Revisited. *NeuroImage* **84**, 971–985 (2014).

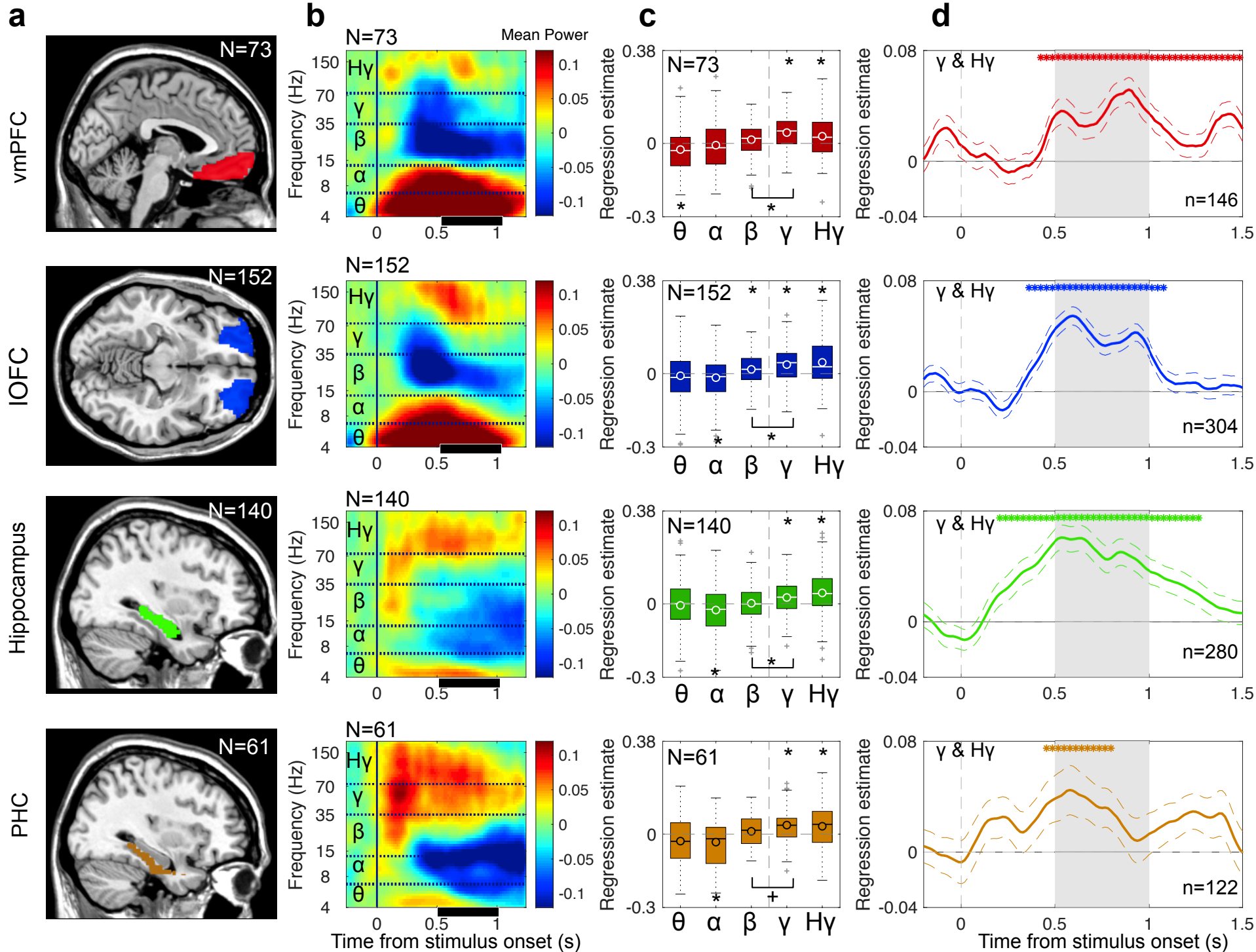
1065 51. Stephan, K. E., Penny, W. D., Daunizeau, J., Moran, R. J. & Friston, K. J. Bayesian model selection for group  
1066 studies. *NeuroImage* **46**, 1004–1017 (2009).

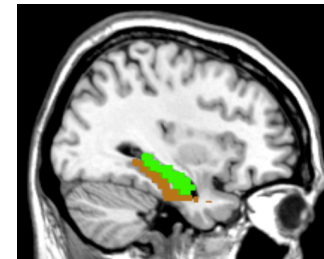
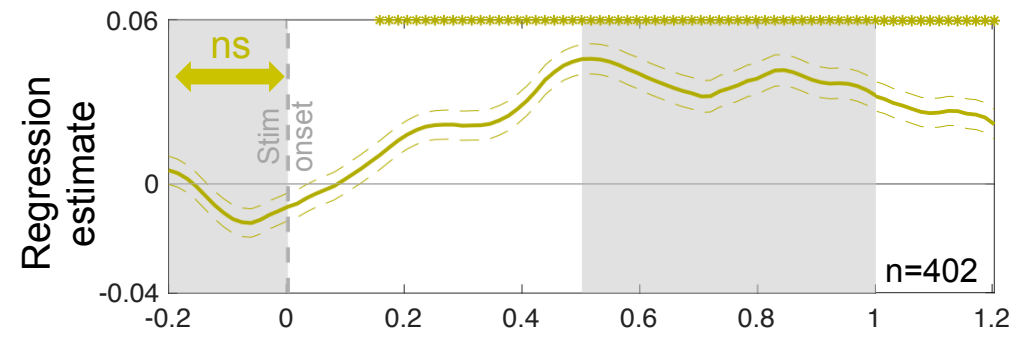
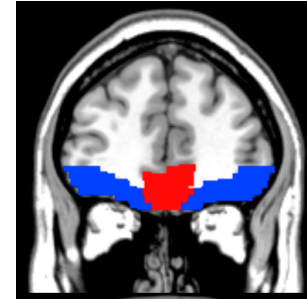
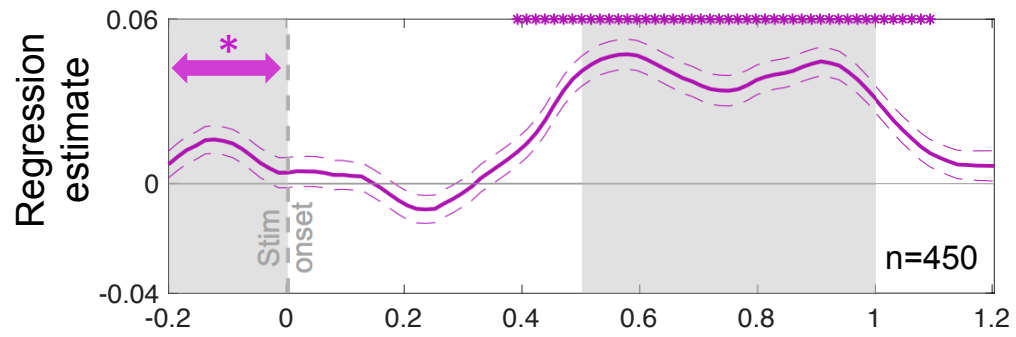
1067 52. Bastin, J. *et al.* Direct Recordings from Human Anterior Insula Reveal its Leading Role within the Error-  
1068 Monitoring Network. *Cereb. Cortex* bhv352 (2016) doi:10.1093/cercor/bhv352.

1069 53. Maris, E. & Oostenveld, R. Nonparametric statistical testing of EEG- and MEG-data. *J. Neurosci. Methods*  
1070 **164**, 177–190 (2007).



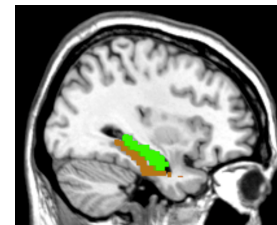
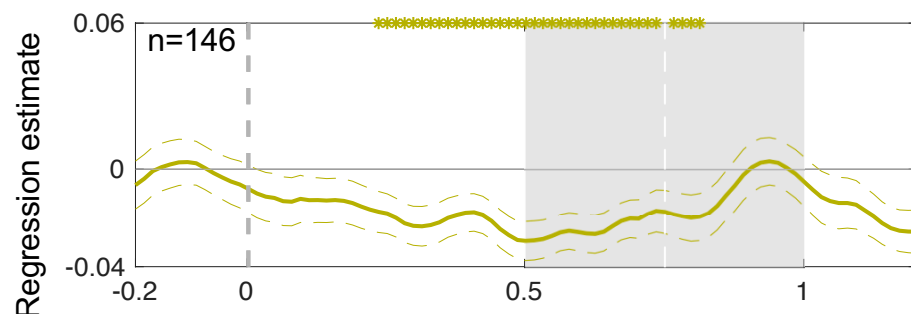
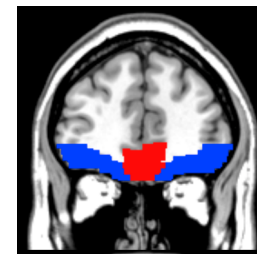
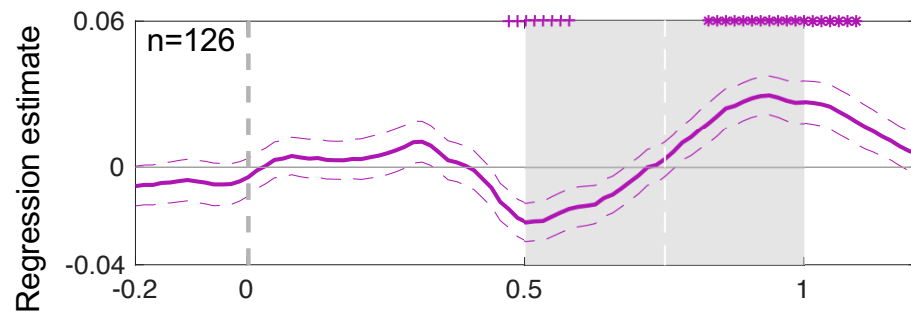
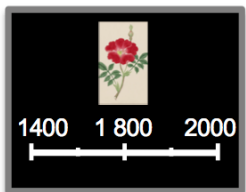
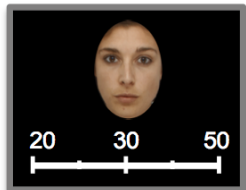




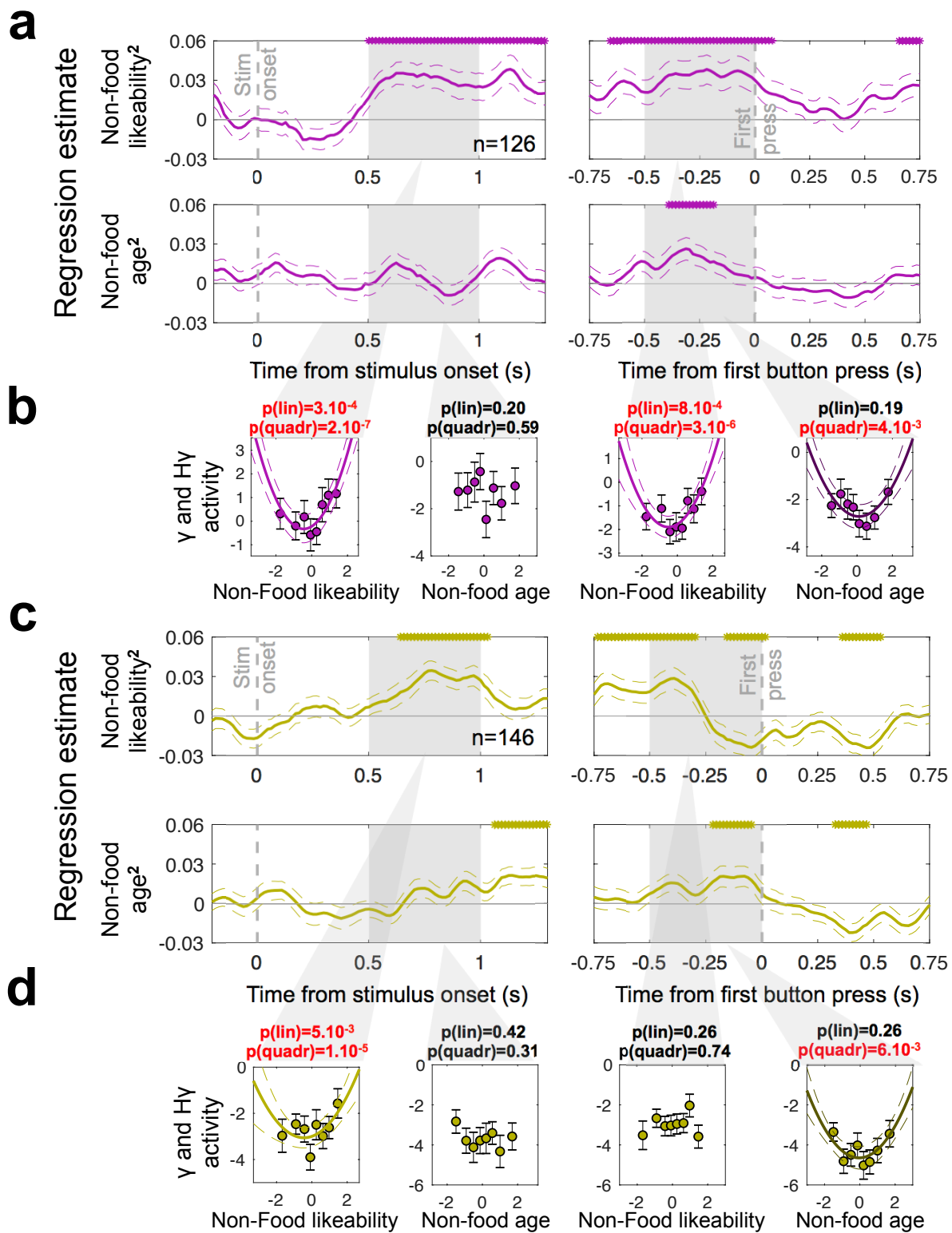


Time from stimulus onset (s)

### Non-food likeability during age rating







Supplementary Table 1: Demographical data

Task version	Recording center	ID	Sex	Age (years)	Epilepsy onset (age)	Suspected Epileptic focus	Intellectual Quotient (IQ)	Hand laterality	Number of electrodes	Number of recording sites	Number of sites in vmPFC	Number of sites in IOFC	Number of sites in Hippocampus	Number of sites in PHC
Complete	Grenoble	G1	M	37	29	Left OFC	NA	NA	13	165	9	10	0	0
Short		G2	F	31	24	Left temporal	100	R	12	156	0	0	6	0
Short		G3	M	47	38	Right temporal	96	R	18	328	4	2	11	2
Short		G4	F	34	26	Right OFC	76	R	16	208	2	6	2	2
Short & Complete		G5	F	47	19	Bi-fronto-temporal	120	R	16	203	2	16	2	2
Short (only rating)		G6	M	57	37	Left anterior temporal	104	NA	12	187	5	5	4	4
Complete		G7	F	39	28	Left temporal	76	R	17	229	2	0	1	6
Short	Lyon	L1	F	49	39	Right temporal	NA	R	14	149	1	6	4	4
Short		L2	M	21	14	Left fronto-temporal	NA	R	15	168	2	6	5	0
Short		L3	F	43	2	Left temporale	NA	R	13	129	2	12	4	0
Short		L4	F	40	15	NA	NA	L	11	109	0	0	9	0
Short		L5	F	38	28	Left temporal	NA	R	9	98	0	0	6	0
Short		L6	M	22	NA	NA	NA	L	11	133	6	8	2	4
Short		L7	F	48	19	Right temporal	NA	R	13	149	2	6	2	2
Short		L8	M	41	NA	Left temporal	NA	L	5	50	1	4	1	0
Short		L9	M	30	NA	Right fronto-temporal	NA	R	13	149	5	4	11	0
Short		L10	F	21	4	Left frontal / insula	NA	R	11	115	2	4	0	0
Short		L11	M	26	21	NA	NA	R	12	132	4	4	8	3
Short		L12	F	43	40	Left temporal	NA	L	13	126	3	2	6	0
Short		L13	F	26	4	Left anterior temporal	NA	R	13	127	3	3	1	0
Short		L14	F	31	NA	NA	NA	R	12	121	2	7	0	0
Short		L15	F	45	21	Left temporal /insula	NA	R	10	110	0	0	9	0
Short		L16	M	44	NA	NA	NA	R	11	114	2	1	2	5
Short		L17	M	48	NA	NA	NA	R	14	153	1	5	0	0
Short		L18	M	51	11	NA	NA	R	12	128	2	7	4	1
Complete	Paris	P1	M	22	7	Left temporal	79	R	9	78	0	5	5	2
Complete		P2	F	55	36	Right temporal	96	R	11	94	2	1	6	4
Complete		P3	F	60	32	Right anterior temporal	89	L	8	57	0	0	10	3
Complete		P4	F	30	16	dorso-medial frontal	117	R	10	66	3	0	0	0
Complete		P5	M	29	20	Right posterior temporal	NA		8	60	0	0	3	0
Complete		P6	F	22	8	dorso-medial frontal	NA	R	10	58	0	0	0	0
Complete		P7	F	34	9	Left Insula / Amygdala	110	R	8	68	1	5	1	1
Complete		P8	F	39	23	Left anterior temporal	106	R	7	62	1	3	4	2
Complete (without faces)		P9	M	34	12	Right anterior temporal	NA	R	10	78	0	0	2	5
Complete		P10	M	37	24	Right anterior temporal	NA	R	7	50	2	4	1	1
Complete		P11	F	45	25	Right temporal	NA	R	9	78	0	0	6	6

IQ: Intellectual Quotient; NA: Missing Data, OFC: Orbito-Frontal Cortex; R: Right, L: Left, Bi: Bilateral; M: Male; F: Female



**Supplementary Table 2: Brain regions obtained from re-parcellation of the AAL atlas**

AAL (restructured) label	N	AAL (restructured) label	N	AAL (restructured) label	N
Temporal Mid L ant/ant	148	Frontal Mid L ant/inf	31	Angular L	8
Temporal Mid L ant/post	119	Frontal Inf Oper L	31	Thalamus R	8
Temporal Sup R ant	117	Frontal Sup Orb R	30	Occipital Mid R sup	8
Temporal Sup L ant	111	Amygdala L	30	Temporal Mid R post/post	7
Hippocampus L	104	Rectus	29	Postcentral R inf/ant	7
Hippocampus R	102	Rolandic Oper R	26	Putamen L	7
Temporal Inf R ant	92	Cingulum Ant R	26	Parietal Inf R	7
Temporal Mid R ant/ant	84	SupraMarginal R	25	Angular R	6
Insula L	82	Frontal Inf Tri R post	25	Cingulum Mid R post	6
Insula R	82	Frontal Mid L post/inf	24	Postcentral R inf/post	6
Temporal Mid R ant/post	80	ParaHippocampal L	23	Parietal Inf L post	5
Frontal Inf Orb R	75	Frontal Mid R post/sup	23	Supp Motor Area R post	4
Frontal Inf Orb L	65	Heschl R	23	Cingulum Post	4
Temporal Inf L ant	57	Postcentral L inf	23	Cuneus R	4
Frontal Mid Orb R	53	Temporal Pole Sup L	22	Precuneus R inf	3
Temporal Sup R post	51	Fusiform L post	22	Frontal Sup Medial L sup	3
Temporal Pole Mid R	51	Frontal Sup R post/ant	21	Lingual R ant	3
ParaHippocampal R	49	Frontal Sup L ant	21	Parietal Sup L ant	3
Frontal Sup R ant	49	Temporal Mid L post/post	21	Precentral R sup	3
Temporal Mid L post/ant	48	Temporal Mid R post/ant	18	Precentral L sup	3
Frontal Mid R ant inf	47	Rolandic Oper L	18	Olfactory	2
Frontal Mid Orb L	45	Frontal Sup Medial R inf	17	Caudate	2
Frontal Med Orb	44	SupraMarginal L	16	Cerebellum L	2
Precentral R inf	43	Cingulum Mid R ant	15	Calcarine R	2
Temporal Sup L post	42	Cingulum Mid L	15	Pallidum R	2
Temporal Inf L post	40	Supp Motor Area R ant	14	Cuneus L	2
Frontal Mid R ant/sup	40	Temporal Inf R post	14	Occipital Sup L	2
Frontal Inf Tri R ant	39	Frontal Sup R post/post	13	Caudate R	2
Frontal Mid L ant/sup	37	Frontal Sup Medial L inf	12	Fusiform R post	2
Frontal Mid R post/inf	37	Frontal Sup L post	12	Paracentral Lobule	2
Fusiform R ant	36	Putamen R	12	Parietal Sup R ant	2
Frontal Inf Oper R	35	Precentral L inf	12	Precuneus L inf	2
Temporal Pole Mid L	34	Frontal Sup Medial R sup	10	Occipital Inf L	1
Frontal Inf Tri L post	34	Lingual L ant	10	Supp Motor Area L ant	1
Cingulum Ant L	34	Heschl L	10	Pallidum L	1
Fusiform L ant	33	Amygdala R	9	Occipital Sup R	1
Temporal Pole Sup R	33	Frontal Mid L post/sup	9	Occipital Mid L ant	1
Frontal Inf Tri L ant	33	Postcentral R sup	9	Precuneus L sup	1
Frontal Sup Orb L	32			NA	235

Inf: inferior; Sup: Superior; Ant: Anterior; Post: Posterior; L: Left; R: Right; Mid: Middle; Med: Median; Tri: Triangularis; Supp: Supplementary; Orb: Orbital; Oper: Opercular.; NA: Not Attributed. Grey: Areas not included in the pseudo whole-brain analysis (less than 9 recorded sites). Red: vmPFC; blue: IOFC; green: hippocampus; orange: PHC. N indicates the number of recording sites.

**Supplementary Table 3: Pseudo whole-brain analysis of food value signaling in a priori high-gamma range (50-150Hz)**

POSITIVE CORRELATION WITH VALUE				
AAL label	Number of sites	Significant sites (%)	max t-value	p-value
Hippocampus L	104	36	291,54	< 5.10 <sup>-4*</sup>
Hippocampus R	102	40	245,32	< 5.10 <sup>-4*</sup>
Frontal Mid Orb L	45	44	133,16	< 5.10 <sup>-4*</sup>
Frontal Sup R ant	49	34	129,83	< 5.10 <sup>-4*</sup>
Temporal Inf L ant	57	28	114,25	< 5.10 <sup>-4*</sup>
Frontal Mid R ant/inf	47	24	110,39	< 5.10 <sup>-4*</sup>
ParaHippocampal L	23	47	107,39	< 5.10 <sup>-4*</sup>
Frontal Sup Orb R	30	37	107,29	< 5.10 <sup>-4*</sup>
Fusiform L ant	33	39	97,33	< 5.10 <sup>-4*</sup>
Fusiform R ant	36	44	79,98	5.10 <sup>-4*</sup>
Frontal Mid Orb R	53	34	77,49	< 5.10 <sup>-4*</sup>
Frontal Med Orb	44	36	77,18	< 5.10 <sup>-4*</sup>
Frontal Inf Tri L ant	33	36	76,97	< 5.10 <sup>-4*</sup>
Frontal Mid L post/sup	9	44	75,1	5.10 <sup>-4*</sup>
ParaHippocampal R	49	27	69,13	< 5.10 <sup>-4*</sup>
Fusiform L post	22	41	62,63	5.10 <sup>-4*</sup>
Frontal Sup Orb L	32	41	60,05	< 5.10 <sup>-4*</sup>
Temporal Pole Sup R	33	39	50,58	2.10 <sup>-3</sup>
Precentral L inf	12	50	49,63	6.10 <sup>-3</sup>
SupraMarginal R	25	44	49,44	5.10 <sup>-4*</sup>
Cingulum Ant L	34	24	43,29	3.10 <sup>-3</sup>
Frontal Inf Oper R	35	26	39,18	4.10 <sup>-3</sup>
Frontal Sup Medial L inf	12	25	37,76	8.10 <sup>-3</sup>
Rectus	29	28	33,35	4.10 <sup>-3</sup>
Temporal Pole Mid L	34	26	31,29	6.10 <sup>-3</sup>
Temporal Mid L ant/ant	148	24	31,14	8.10 <sup>-3</sup>
Temporal Mid R ant/post	80	28	30,71	8.10 <sup>-3</sup>
Cingulum Ant R	26	23	30,38	8.10 <sup>-3</sup>
Temporal Inf R ant	92	27	30,2	8.10 <sup>-3</sup>
Frontal Inf Tri R post	25	24	29,74	9.10 <sup>-3</sup>
Temporal Inf L post	40	25	27,3	0,01
Temporal Mid R post/ant	18	33	25,12	0,02
Cingulum Mid L	15	33	21,33	0,02
Frontal Inf Oper L	31	26	13,95	0,04
Insula L	82	23	13,26	0,049

NEGATIVE CORRELATION WITH VALUE			
AAL label	Number of sites	max t-value	p-value
Heschl R	23	-159,21	< 5.10 <sup>-4*</sup>
Heschl L	10	-124,58	< 5.10 <sup>-4*</sup>
Postcentral R sup	9	-107,97	< 5.10 <sup>-4*</sup>
Temporal Sup R ant	117	-103,31	< 5.10 <sup>-4*</sup>
Frontal Mid R post sup	23	-81,31	< 5.10 <sup>-4*</sup>
Precentral R inf	43	-62,37	5.10 <sup>-4*</sup>
Temporal Sup L ant	111	-59,21	5.10 <sup>-4*</sup>
Frontal Mid L ant inf	31	-39,33	0.0025*
Amygdala R	9	-27,91	0,014
Temporal Sup R post	51	-24,38	0,017
Frontal Mid R post inf	37	-23,47	0,0135
Cingulum Mid R ant	15	-22,1	0,027
Frontal Inf Tri R ant	39	-20,53	0,024

Same abbreviations as in Supplementary Table 2. Areas are ordered according to the maximal t-value obtained at cluster level in the regression of high-gamma activity against food likeability rating. Red: vmPFC; blue: IOFC; green: hippocampus; orange: PHC, grey: significant bilateral regions included in the extended BVS. p-values are obtained with two-sided one-sample t-tests cluster-wise corrected (p<0.05). Stars indicate significance after Bonferroni-Holm correction for multiple comparisons across regions.

**Supplementary Table 4: Pseudo whole-brain analysis of food value signaling in a priori gamma range (35-50Hz)**

POSITIVE CORRELATION WITH VALUE			
AAL label	Number of sites	max t-value	p-value
Frontal Inf Tri L post	34	87,75	< 5.10 <sup>-4</sup> *
Frontal Inf Orb L	65	80,43	< 5.10 <sup>-4</sup> *
Frontal Med Orb	42	61,51	0.001*
Frontal Sup R ant	49	54,97	0.0005*
Frontal Inf Oper R	35	53,76	0.0015*
Frontal Inf Tri L ant	33	43,63	0.003*
Frontal Mid Orb L	45	34,99	0,015
Temporal Sup R post	45	33,36	0,018
Frontal Mid L ant/inf	31	33,08	0,0155
Cingulum Ant L	34	32,91	0,016
Rolandic Oper L	18	31,42	0,022
Frontal Mid L post/sup	9	30,78	0,039
Frontal Mid Orb R	53	25,02	0,048

NEGATIVE CORRELATION WITH VALUE			
AAL label	Number of sites	max t-value	p-value
Postcentral L inf	23	-43,61	0.004*
Rolandic Oper R	21	-42,06	0.009*
Frontal Mid R post/inf	36	-35,05	0.0135*
Frontal Inf Tri R ant	39	-34,11	0.017*

Same legend as in Supplementary Table 3. Areas are ordered according to the maximal t-value obtained at cluster level in the regression of gamma activity against food likeability rating. p-values are obtained with two-sided one-sample t-tests cluster-wise corrected (p<0.05).

**Supplementary Table 5: Pseudo whole-brain analysis of food value signaling in a priori beta range (15-35Hz)**

POSITIVE CORRELATION WITH VALUE			
AAL label	Number of sites	max t-value	p-value
Frontal Sup Medial R sup	10	67,66	0.001*
Temporal Sup L ant	111	63,69	0.001*
Temporal Sup L post	42	55,01	0.0025*
Temporal Mid R ant/ant	84	54,08	0.0045*
Frontal Sup R post/ant	21	52,94	0.0045*
Frontal Mid R ant/sup	40	46,76	0,007
Frontal Sup Orb L	32	41,41	0,013
Temporal Mid R ant/post	80	39,55	0,017
Hippocampus R	102	34,99	0,0215
Frontal Mid Orb R	53	33,79	0,0155
Frontal Inf Tri L post	34	33,01	0,029
Frontal Sup R post/post	13	32,85	0,035
Frontal Mid Orb L	45	27,61	0,048
Temporal Mid L ant/ant	148	27,05	0,0455

NEGATIVE CORRELATION WITH VALUE			
AAL label	Number of sites	max t-value	p-value
Temporal Mid L post/post	21	-140,8	$< 5.10^{-4}$ *
Temporal Mid L ant/post	119	-107,3	$< 5.10^{-4}$ *
Precentral L inf	12	-91,45	$< 5.10^{-4}$ *
Temporal Mid L post/ant	48	-86,63	$< 5.10^{-4}$ *
Temporal Inf L post	40	-72,3	$< 5.10^{-4}$ *
Cingulum Mid L	15	-63,37	0.001*
Temporal Sup R post	51	-54,2	0.0035*
Precentral R inf	43	-53,04	0.0035*
SupraMarginal L	16	-40,79	0,026
Temporal Sup R ant	117	-36,38	0,0205
Frontal Mid L post/sup	9	-35,89	0,032
Temporal Pole Mid R	51	-35,6	0,034
Amygdala R	9	-35,18	0,043
Frontal Mid R post/sup	23	-33,39	0,0255
Postcentral L inf	23	-30,97	0,035
Frontal Inf Tri R ant	39	-29,65	0,0325

Same legend as in Supplementary Table 3. Areas are ordered according to the maximal t-value obtained at cluster level in the regression of beta activity against food likeability rating. p-values are obtained with two-sided one-sample t-tests cluster-wise corrected ( $p < 0.05$ ).

**Supplementary Table 6: Pseudo whole-brain analysis of food value signaling in a priori alpha range (8-15Hz)**

POSITIVE CORRELATION WITH VALUE			
AAL label	Number of sites	max t-value	p-value
Frontal Sup Medial R sup	10	335,35	$< 5.10^{-4} *$
Temporal Sup L post	42	274,59	$< 5.10^{-4} *$
Temporal Sup L ant	111	193,29	$5.10^{-4} *$
Frontal Sup R post/post	13	184,74	0.001*
Supp Motor Area R ant	14	90,21	0,024
Frontal Sup R ant	49	86,1	0,019
Rolandic Oper R	21	77,15	0,029

NEGATIVE CORRELATION WITH VALUE			
AAL label	Number of sites	max t-value	p-value
Frontal Mid L post inf	24	-275,05	$< 5.10^{-4} *$
Frontal Sup L post	12	-255,51	$< 5.10^{-4} *$
Temporal Mid L post/ant	48	-209,09	$< 5.10^{-4} *$
Temporal Pole Mid L	34	-166,33	$< 5.10^{-4} *$
Frontal Inf Tri R post	25	-159,54	0.0035*
Temporal Inf L post	40	-153,7	$5.10^{-4} *$
Hippocampus R	82	-153,63	0.0025*
Frontal Inf Tri L post	34	-146,89	0.0015*
Cingulum Mid L	15	-126,21	0,007
Temporal Pole Mid R	45	-124,75	0,007
Temporal Mid L post/post	21	-122,76	0,013
Frontal Mid L ant inf	31	-114,33	0,006
Frontal Mid L post sup	9	-112,01	0,013
Fusiform L post	22	-108,37	0,007
Temporal Mid L ant/post	119	-97,21	0,015
Frontal Sup Orb R	29	-79,55	0,029
Temporal Sup R post	45	-78,93	0,029
Precentral R inf	43	-75,22	0,043
Hippocampus L	105	-73,99	0,025
SupraMarginal L	16	-67,09	0,039

Same legend as in Supplementary Table 3. Areas are ordered according to the maximal t-value obtained at cluster level in the regression of alpha activity against food likeability rating. p-values are obtained with two-sided one-sample t-tests cluster-wise corrected ( $p < 0.05$ ).

**Supplementary Table 7: Pseudo whole-brain analysis of food value signaling in a priori theta range (4-7Hz)**

POSITIVE CORRELATION WITH VALUE			
AAL label	Number of sites	max t-value	p-value
Temporal sup L post	42	227,21	< 5.10 <sup>-4</sup> *
Frontal sup R post/ant	21	198,77	0.001*
Temporal inf R post	14	121,89	0.003*
Frontal sup Medial R sup	10	108,07	0,015
Putamen R	12	73,73	0,045
Frontal Mid R ant sup	40	72,86	0,031
Cingulum Mid L	15	62,95	0,042
Temporal Pole sup L	22	62,01	0,047

NEGATIVE CORRELATION WITH VALUE			
AAL label	Number of sites	max t-value	p-value
Frontal Mid L post inf	24	-297,66	< 5.10 <sup>-4</sup> *
Frontal sup L post	12	-292,35	< 5.10 <sup>-4</sup> *
Frontal inf Tri R post	25	-240,08	< 5.10 <sup>-4</sup> *
Frontal inf Oper L	31	-229,31	5.10 <sup>-4</sup> *
Frontal inf Tri L ant	33	-189,11	5.10 <sup>-4</sup> *
Frontal Mid Orb L	45	-169,32	0.001*
Temporal Mid R ant/post	68	-152,1	0.001*
Frontal Mid L ant inf	31	-127,85	0,004
supraMarginal L	16	-127,16	0,003
Temporal Mid L post/ant	48	-125,47	0,004
Precentral L inf	12	-120,72	0,007
Frontal inf Tri R ant	39	-116,39	0,007
postcentral L inf	23	-115,26	0,007
Temporal Pole Mid L	34	-114,85	0,006
Temporal Mid L ant/ant	148	-110,47	0,011
Frontal Mid Orb R	53	-105,93	0,013
Precentral R inf	43	-103,15	0,012
Frontal inf Orb L	65	-94,21	0,019
Temporal sup R post	45	-87,12	0,015
Rectus combined	29	-85,67	0,022
Fusiform R ant	34	-78,73	0,026
Frontal inf Tri L post	34	-78,63	0,02
Frontal Mid R ant inf	47	-78,48	0,026
Temporal sup R ant	95	-76,23	0,025
Frontal inf Orb R	68	-66,9	0,04
Temporal inf R ant	79	-65,44	0,035
ParaHippocampal L	23	-60,59	0,047

Same legend as in Supplementary Table 3. Areas are ordered according to the maximal t-value obtained at cluster level in the regression of theta activity against food likeability rating. p-values are obtained with two-sided one-sample t-tests cluster-wise corrected ( $p < 0.05$ ).

**Supplementary Table 8: Functional properties in the supplementary BVS areas**

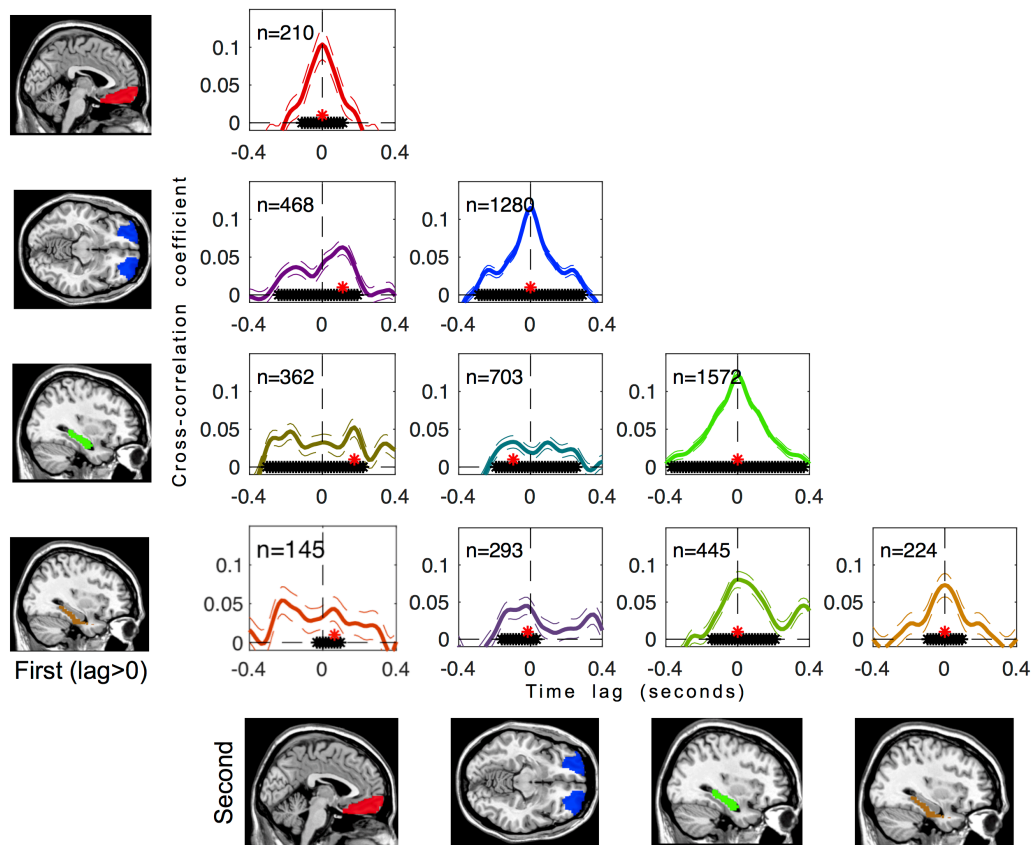
		ANTICIPATION	GENERICITY	AUTOMATICITY		QUADRATICITY
				0.5 – 0.75s	0.75 – 1s	
Temporal inferior	n	298	126	126	126	298
	mean	-0,006	-0,022	-0,001	0,009	0,019
	SEM	0,004	0,006	0,009	0,008	0,005
	df	297	127	127	127	297
	t	-1,267	-3,362	-0,088	1,11	4,064
	p	0,206	<b>0,001</b>	0,93	0,269	<b>6.10<sup>-5</sup></b>
Fusiform anterior	n	88	64	64	64	88
	mean	0,008	-0,007	-0,027	-0,003	0,028
	SEM	0,009	0,009	0,011	0,01	0,008
	df	87	65	65	65	87
	t	0,976	-0,771	-2,448	-0,342	3,45
	p	0,332	0,443	<b>0,017</b>	0,733	<b>0,001</b>
Cingulate	n	94	14	14	14	94
	mean	0,004	0,02	-0,001	-0,011	0,016
	SEM	0,007	0,011	0,019	0,017	0,008
	df	93	15	15	15	93
	t	0,586	1,815	-0,061	-0,644	2,011
	p	0,56	0,09	0,952	0,529	<b>0,047</b>
Frontal inferior opercularis	n	66	38	38	38	66
	mean	0,001	0,017	-0,029	-0,008	-0,036
	SEM	0,011	0,014	0,017	0,013	0,012
	df	65	39	39	39	65
	t	0,08	1,22	-1,771	-0,581	-3,062
	p	0,937	0,23	0,084	0,565	<b>0,003</b>

Summary statistics for each functional property in the supplementary BVS regions (two-sided one-sample Student's test). Abbreviations: SEM: Standard error of the mean; df: degree of freedom; t: t-value; p: p-value; n: number of power time series included in the analysis. In bold are the significant results. Anticipation: test of the food likeability regression estimates on the -0.2-0s time window before stimulus onset. Genericity: test of the non-food likeability regression estimates on the 0.5-1.0s time window after stimulus onset. Automaticity: test of the non-food likeability regression estimates during the age-rating task on the 0.5-0.75s and 0.75-1.0s time windows after stimulus onset. Quadraticity: test of the food likeability squared rating regression estimates during the food likeability rating task on the -0.5-0s time window before response onset.

# Four core properties of the human brain valuation system demonstrated in intracranial signals

## Supplementary information

Supplementary Figure 1 – Temporal dependencies of value signals across brain regions



To better specify the propagation of value signals across time during food likeability rating trials, we conducted a cross-correlation analysis between the high-gamma regression estimates of all possible within-subject pairs of recording sites in BVS regions.

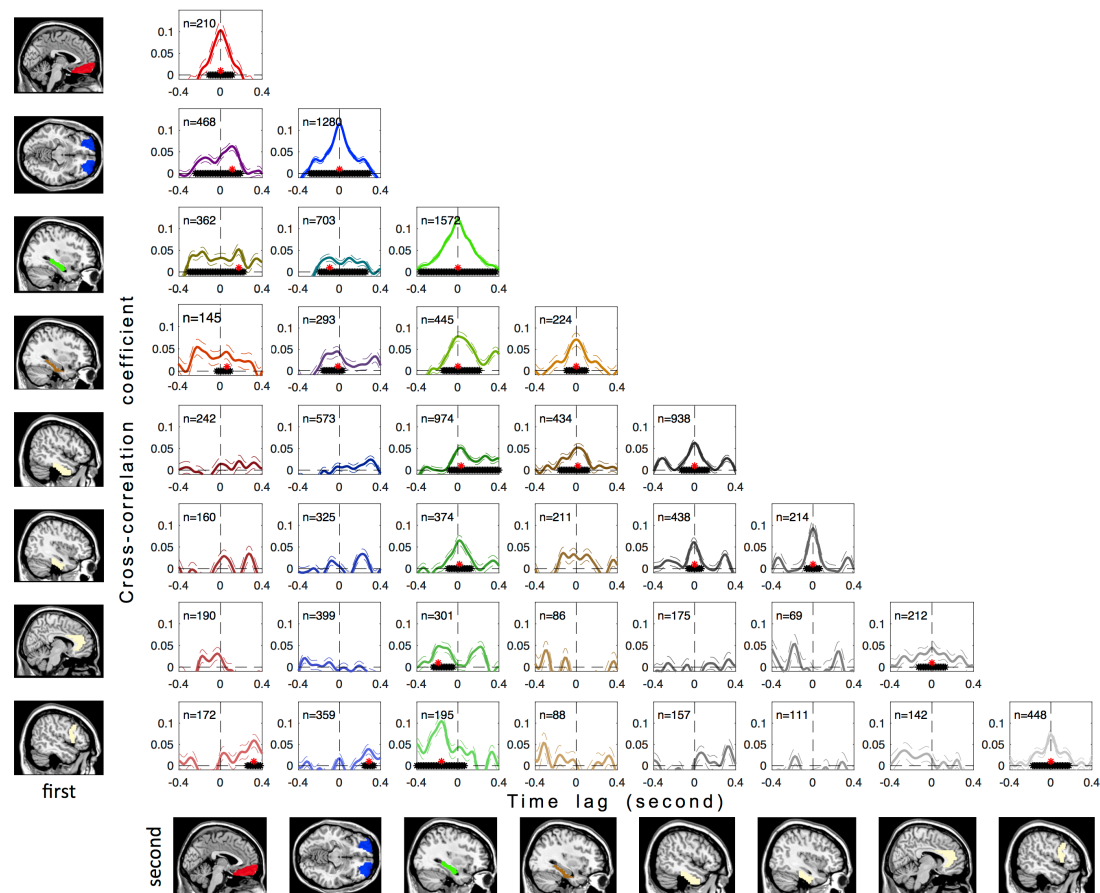
Plots show pairwise Pearson's correlation coefficient of regression estimates (food likeability rating regressed against high-gamma activity) between regions of interest, calculated across trials for every time point. Black stars indicate significant correlations (two-sided one-sample t-test,  $p < 0.05$ , cluster corrected), red stars point to the peaks of significant correlations.  $n$  is the number of within-subject pairs of recording sites included in the correlation analysis. Regions: vmPFC (red), IOFC (blue); hippocampus (green); PHC (brown). The color of cross-correlograms is a mixture of the two colors of correlated brain regions (e.g., purple for vmPFC and IOFC). Solid (and dashed) lines indicates mean (and SEM) across  $n$  pairs of recording sites.

This analysis revealed that all pairs were significantly correlated, with variable time-lags. First, the pairs located within each ROI showed significant correlation with a mean



time-lag of zero, suggesting that value signals emerged at about the same time across the contacts situated in a same BVS region. Second, vmPFC value signals appeared later (mean lag of 112ms) than IOFC signals. Third, there was no significant time-lag between hippocampus and PHC regions, which were thus signaling value simultaneously. The time-lags between OFC and (P)HC regions must be taken with caution, as there was no clear correlation peak. The presence of correlation peaks at both negative and positive time-lags could reflect a two-way exchange of value-related information between ROIs.

### Supplementary Figure 2 – Temporal dependencies of value signals across brain regions in the extended BVS



The analysis is identical to that illustrated in the previous figure, but it now includes every region of the extended BVS.

Plots show pairwise Pearson's correlation coefficients of regression estimates (food likeability rating regressed against high-gamma activity) between regions of interest, calculated across trial for every time point. Positive time lag indicates that the region in rows (first) precedes the region in columns (second). Black stars indicate significant correlations (two-sided one-sample t-test,  $p < 0.05$ , cluster corrected), red stars point to the peaks of significant correlations.  $n$  is the number of within-subject pairs of recording sites included in the correlation analysis. Regions of the BVS: vmPFC (red), IOFC (blue); hippocampus (green); PHC (brown). The color of cross-correlograms is a mixture of the two colors of correlated brain regions (e.g., purple for vmPFC and

IOFC). Regions of the extended BVS are shown in yellow (from left to right, and top to bottom: inferior temporal cortex, fusiform anterior gyrus, anterior cingulate gyrus and opercular part of the inferior frontal gyrus). Solid (dashed) lines indicates mean (SEM) across pairs of recording sites.